Post-print of: Zbigniew Czaja, Time-domain measurement methods for R, L and C sensors based on a versatile direct sensor-to-microcontroller interface circuit, Sensors and Actuators A: Physical, Volume 274, 2018, Pages 199-210, https://doi.org/10.1016/j.sna.2018.03.029.

Time-domain measurement methods for R, L and C sensors based on a versatile direct sensor-to-microcontroller interface circuit

Zbigniew Czaja

Gdansk University of Technology,
Faculty of Electronics, Telecommunications and Informatics,
Department of Metrology and Optoelectronics,
ul. G. Narutowicza 11/12, 80-233 Gdansk, Poland,
email: zbczaja@pg.edu.pl.

Abstract

In the paper new time-domain measurement methods for determining values of resistive (R), inductive (L) and capacitive (C) sensors based on a versatile direct sensor-to-microcontroller interface for microcontrollers with internal analog-to-digital converters (ADCs) and analog comparators (ACs) are presented. The interface circuit consists of a reference resistor R_r working as a voltage divider, a given R, L or C sensor and a microcontroller (its peripherals: an ADC, an AC, a timer, I/O pins buffered by an inverter). A prototype of the proposed complete solution of a compact smart sensor based on an 8-bit microcontroller has been developed and tested. The maximum possible relative inaccuracy of an indirectly measurable resistance, inductance and capacitance were analysed. Also, experimental researches were made. The following relative errors of the sensor value determination were achieved: for the R sensor less than 3%, as well as very good results for the L sensor (less than 0.3%) and for the C sensor (less than 0.2%).

Keywords: microcontroller interfacing, impedance sensors, ADCs, time-domain measurement

1. Introduction

Smart sensors are used inter alia in industrial control and automation, automotive industry and consumer, medical and military applications. They are usually built into the devices and in such cases they are parts of the control systems of these devices (e.g. in automotive applications). Also, they can work as independent devices (e.g. as wearable electronics in customer or medical applications and as environment monitoring sensors). They measure physical variables of the monitored environment, objects and processes (e.g. temperature, ambient humidity, pressure and tension), process and store the measurement data and often they send these data via any wireless interface to a smartphone, tablet, PC or to the main controller of the monitored device. Smart

sensors consist of analog or digital sensors, conditioning circuits, processing and control units and communication interfaces.

In many cases smart sensors are battery-powered or their power supply is based on the energy harvesting technique [1]. Therefore, they should be energy-efficient data acquisition systems, and, ideally, they should be small and cheap [2]. For these reasons, universal sensor interface chips, e.g. [3,4], smart sensor modules based on two-terminal or four-terminal methods, e.g. [5-8], are too expensive and too complex. However, these requirements can be satisfied by the use of widely available low-power one-chip universal devices (i.e. the microcontrollers) as control units. An additional advantage of microcontrollers is that they can convert analog information provided by analog sensors via conditioning circuits to the digital form which next they can also process, store and send.

Important groups of analog sensors are resistive (*R*), inductive (*L*) and capacitive (*C*) sensors. These sensors can be arranged in the form of a single-element, a differential configuration or a bridge configuration. To obtain such low-cost and low-power solutions for resistive sensors [9-13], differential resistive sensors [14], resistive sensors bridges [15,16], inductive sensors [17], capacitive sensors [18,19], differential capacitive sensors [20] based on microcontrollers - the direct sensor-to-microcontroller methods were developed.

The task of such direct interface circuits is to measure the discharging time of either an *RC* network consisted of resistances or capacitances of the sensor or an *RL* network consisted of inductance of the sensor. It was noticed that the parameters of the microcontroller pins, which depend on the manufacturing technology, have a noticeable impact on the measurement accuracy. To eliminate it a direct sensor-to-microcontroller interface circuit was extended with additional components, e.g. a calibration resistor [21], MOSFET transistors [22,23], or also an inverter consisted of two MOSFET transistors [24].

In the cited methods [8-23] only digital input/output pins and internal timers/counters of the microcontrollers are used to determine values of resistance, inductance or capacitance of the sensors. However, nowadays almost all modern 8-bit and especially 32-bit microcontrollers are likewise equipped with analog-to-digital converters (ADCs) and also analog comparators (ACs).

Thus, new time-domain measurement methods for determining values of *R*, *L* and *C*, based on a direct sensor-to-microcontroller interface for microcontrollers with internal ADCs and ACs are proposed in the paper. It should be emphasized that for measurements of *R*, *L* and *C* components there is used only one common hardware configuration of the interface circuit (Fig. 1) consisting of a reference resistor R_r working as a voltage divider [25], a given sensor and a microcontroller (more precisely its peripherals: an ADC, an AC, a timer, I/O pins buffered by an inverter [26] (Fig. 2)). The differences between measurement methods for respective components exist exclusively in the

microcontroller software. Additionally, an advantage of the proposed solution is its hardware and software simplicity, and also a short measurement time, what results in a low-cost, low-power solution of the sensor interface circuit.

Hence, the approach can be used to design smart sensors (Fig. 1), and also, which is its greatest asset, it can be used in easy and cheap way of extending the functionality of existing systems based on microcontrollers.

The paper is organized as follows: Section 2 presents the operating principle of the interface circuit for measurements of *R*, *L* and *C*, Section 3 analyses the error sources of these measurements and their limitations, Section 4 describes experimental results and proposals to improve measuring accuracy, and Section 5 contains the main conclusions.

2. Operating principle

The proposed direct interface circuit for *R*, *L* and *C* sensors is shown in Fig. 2. An impedance *Z* represents one of the *R*, *L* or *C* sensors. A reference resistor R_r works as a current-to-voltage converter [25,26] and together with the impedance *Z* acts as a voltage divider. An inverter consisted of only two MOSFETs [27] buffers the output pin of the microcontroller [25].

The microcontroller, and more precisely its internal measurement peripherals, works simultaneously as a signal generator stimulating the direct interface by a square pulse v_{in} with an amplitude set *a priori* to the supply voltage of the microcontroller V_{CC} , and as a voltage measurement block sampling the voltage response v_{out} of the sensor by the ADC. For *L* and *C* measurements the AC is used to determine an appropriate voltage level at which the ADC samples the voltage response v_{out} and the timer specifies the moment t_m of this sample V_m relative to the beginning of the signal v_{in}. For *R* measurements only the ADC is used.

The proposed approach will be shown on an example of a modern 8-bit ATXmega32A4 microcontroller [28]. An 8-bit microcontroller should be chosen, because each application which can run on 8-bit microcontrollers can also run on 32-bit microcontrollers, what makes the proposed solution versatile. Additionally, it seems that its measurement peripherals are better than in some 32-bit microcontrollers. The only limitation is the fact that the maximum value of the signal v_{out} should be less than a reference voltage V_{ref} of the ADC ($V_{ref} = V_{CC} - V_D$, $V_D \approx 0.7$ V and $V_{CC} =$ 3.3 V), i.e. its values should be within the measurement range of the ADC.

The smart sensor solution based on this microcontroller is shown in Fig. 3. The output pin PC0 is used to set the stimulation signal v_{in}, and the response signal v_{out} at the input ADC 1 is simultaneously applied to the AC input and the ADC input. The threshold voltage value V_{CC_SCALED} of the AC is set by the software.

A divider's voltage ratio $K(s)$ of the direct sensor-to-microcontroller interface circuit (the voltage divider consisting of R_r and Z) is following (1):

$$K(s) = \frac{Z(s)}{Z(s) + R_r}, \tag{1}$$

where

$$K(s) = \frac{v_{out}(s)}{v_{in}(s)} \tag{2}$$

From (1) and (2) we can derive the formula for v_{out} (3):

$$v_{out}(s) = v_{in}(s) \cdot \frac{Z(s)}{Z(s) + R_r} \tag{3}$$

The stimulating signal of the sensor interface circuit v_{in} in the time domain can be written:

$$v_{in}(t) = V_{in} \cdot \left(\mathbf{1}(t) - \mathbf{1}(t - T)\right), \tag{4}$$

where T is a pulse duration, and $V_{in} = V_{CC}$ is a pulse amplitude.

Because all measurements will be carried out only during the pulse duration T, we can simplify (4) to the form:

$$v_{in}(t) = V_{in} \cdot \left(\mathbf{1}(t)\right) \quad \text{for} \quad t \in (0; T) \tag{5}$$

what gives in the frequency domain the simple formula for v_{in}:

$$v_{in}(s) = V_{in} \cdot \frac{1}{s} \tag{6}$$

The formulas (3) and (6) will be the basis for formulas used to determine values of R, L and C sensors.

2.1. Measurements of R sensors

Thanks to using such a simple sensor-to-microcontroller interface circuit, the determination of the R sensor value R_m is easy. In this case - according to (5) - we can assume that during the measurements the resistive divider is stimulated by the DC voltage V_{in}. Hence, the ADC samples the DC voltage response V_{out}. The values R_r and V_{in} are fixed, so we can calculate the R_m value from (7):

$$R_m = R_r \cdot \frac{V_{out}}{V_{in} - V_{out}} \quad \text{where} \quad V_{in} > V_{out} \qquad (7)$$

However, we should remember that the ADC measures instantaneous voltage values, which are disturbed by, among others, working digital circuits and oscillators of the microcontroller. We can minimize the effect of these disturbances on voltage measurements, e.g. by using the method of oversampling. In this case the time T needed for voltage measurement by the ADC is equal to

$$T = t_d + m \cdot t_{ADC} \ , \qquad (8)$$

where t_d – a time delay needed to stabilize the DC voltage, t_{ADC} – an ADC conversion time, m – the number of voltage samples ($m = 4^k$, $k = 0, 1, 2, 3 \ldots$ [29]).

For instance, for the ATXmega32A4 microcontroller, 12-bit ADC resolution [28] and $m = 4$ the voltage measurement takes about $T = 27$ μs.

An important problem is the selection of a resistor value R_r. The value depends on an established range of resistance value changes (from R_{m_min} to R_{m_max}) of the sensor R_m and limitations of the ADC. The first limitation is the reference voltage V_{ref} value, which is less than or equal to V_{CC}, and the second one follows from the fact that measurements of small voltage values are loaded with large measurement errors. Hence, $V_{out} \geq \rho \cdot V_{ref}$, where we can assume that e.g. $\rho = 0.1$. Based on these facts we can write:

$$\frac{R_{m\_\max}}{R_{m\_\max} + R_r} \leq \frac{V_{ref}}{V_{CC}} \quad \text{and} \quad \frac{R_{m\_\min}}{R_{m\_\min} + R_r} \geq \frac{\rho \cdot V_{ref}}{V_{CC}} \qquad (9)$$

what after transformations gives the formulas for a range of values of R_r:

$$\begin{cases} R_r \geq R_{m\_\max} \cdot \dfrac{V_{CC} - V_{ref}}{V_{ref}} \\ R_r \leq R_{m\_\min} \cdot \dfrac{V_{CC} - \rho \cdot V_{ref}}{\rho \cdot V_{ref}} \end{cases} \qquad (10)$$

Therefore, if we plan to use e.g. a resistance sensor Pt1000 [30] for the ATXmega32A4 microcontroller, the minimum values of R_r are following: for a temperature range to 200°C R_{r_min} = 457 Ω, for a range to 600°C R_{r_min} = 813 Ω, and for a range to 850°C R_{r_min} = 1013 Ω. The maximum values of R_r for $\rho = 0.1$ are following: for a range from -200°C R_{r_max} = 2165 Ω, and for a range from -50°C R_{r_max} = 9390 Ω.

2.2. Measurements of L sensors

In this case the impedance Z is represented by the serial connection of a resistance R_s and an inductance L of the coil. It is assumed that the value of resistance R_s is constant and known, and only the values of sensor inductance L representing the measured physical values are changed [31]. Hence, the divider's voltage ratio $K(s)$ of the inductive sensor-to-microcontroller interface circuit is following:

$$K(s) = \frac{sL + R_s}{sL + (R_s + R_r)} \tag{11}$$

Based on (2), (3), (6) and (11) we obtained the formula for $v_{out}(s)$:

$$v_{out}(s) = V_{in} \cdot \left(\frac{1}{s + \frac{R_s + R_r}{L}} + \frac{R_s}{R_s + R_r} \cdot \frac{1}{s\left(s\frac{L}{R_s + R_r} + 1 \right)} \right) \tag{12}$$

In the time domain it has the form:

$$v_{out}(t) = V_{in} \cdot \left(\frac{R_s}{R_s + R_r} + \frac{R_r}{R_s + R_r} \cdot e^{-t \cdot \frac{R_s + R_r}{L}} \right) \text{ for } t \in (0; T) \tag{13}$$

The ADC samples the signal $v_{out}(t)$ at a sample moment t_m determined by the timer of the microcontroller. It takes place when the $v_{out}(t)$ reaches the value V_{cc_scaled}. That is the ADC voltage sample value $V_m = v_{out}(t_m)$, as shown in Fig. 4.

Hence, based on the known values R_s and R_r and the measured values t_m and V_m the value L can be calculated from the following formula:

$$L = \frac{-t_m \cdot (R_s + R_r)}{\ln\left(\frac{\frac{V_m}{V_{in}}(R_s + R_r) - R_s}{R_r} \right)}, \tag{14}$$

where $V_{in} > V_m$ and $R_r > R_s$.

The timing of the measurement procedure for L measurements is shown in Fig. 4. The sensor interface is stimulated by a square pulse v_{in} with an amplitude V_{in} and duration T. The timer is started when the pulse starts. When the voltage response v_{out} decreases to the threshold voltage level V_{cc_scaled}, the AC triggers both the ADC and reading the current value from the timer simultaneously

(Fig. 2 and Fig. 3). The duration of pulse v_{in}, i.e. the duration of measurement procedure, is as short as possible, because $T = t_m + t_{ADC}$, what reduces the energy consumption.

The AC is used only to determine the voltage level at which the ADC accurately samples the response v_{out}. It follows from the fact that ACs included in microcontrollers are not accurate. E.g. a typical input offset voltage of the AC in the ATXmega32A4 microcontroller is less than ±10 mV, and the 6-bit V_{CC} voltage scaler used to set V_{cc_scaled} value in the AC is non-linear [28].

Before measurements, we should determine the threshold voltage level V_{cc_scaled} and the value R_r which will provide the best possible measurement accuracy of t_m and V_m.

The range of observable changes of the voltage v_{out} is contained in a range from V_{ref} down to $V_{in} \cdot R_s/(R_s + R_r)$ (see Fig. 4). Hence, if the value R_r is greater this voltage range is also grater. Thanks to this a value of L has a decisive influence on the voltage v_{out} (13). That means that the value of R_r at least should be greater than the value of R_s. It would be best if $R_r >> R_s$. However, the greater the value R_r the smaller the value t_m, what undesirably affects the accuracy of measurements of time t_m by the timer [32,33]. However, we should remember that R_r plays also the role of a current limiter, hence its value should not be too small.

If we know the range of inductance value changes (from L_{min} to L_{max}) and the value of R_s of L sensor, and we have established the threshold voltage level V_{cc_scaled} value (it will be discussed below) we can assess the value R_r by placing it in the formula (15) and checking whether t_m is greater than the fixed minimum value t_{m_min}.

$$t_m = \frac{-\ln\left(\left(\frac{V_{cc\_scale}}{V_{in}}\left(R_s + R_r\right) - R_s\right) \Big/ R_r\right) \cdot L_{min}}{R_s + R_r} \qquad (15)$$

Because we use the timer to measure time t_m, we can write $t_{m\_min} = N_{min} \cdot T_{clk}$, where N_{min} – the minimum number of internal pulses counted by the timer, T_{clk} – a period of the system clock of microcontroller clocking the timer. Hence, this value is determined by the maximum value of frequency $f_{clk} = 1/T_{clk}$ of the external crystal oscillator, which can be used for a given microcontroller (16 MHz for the ATXmega32A4 [28]), and the number of counted pulses N_{min}. Therefore, the value N_{min} should be as large as possible, because it has a major impact on the measurement errors of time t_m. For instance, if we assume that the measurement errors should be less than 1%, the number $N_{min} = 100$. In this case, for the ATXmega32A4, the time $t_{m\_min} = 6.25$ µs. This time limits the measurement capabilities of a given microcontroller, i.e. the minimum value of inductance which can be measured by the microcontroller with a given crystal oscillator.

A threshold voltage level V_{cc_scaled} value should be set to half of the range of observable changes of the voltage v_{out}, that is:

$$V_{cc\_scaled} = V_{in} \cdot \frac{2 \cdot R_s + R_r}{2 \cdot (R_s + R_r)} \square\square, \qquad (16)$$

where $R_r > R_s$ and $V_{cc\_scaled} < V_{ref}$

For this value the maximum relative measurement error of the voltage v_{out} is the smallest, as it will be explained in Section 3.2.

2.3. Measurements of C sensors

The divider's voltage ratio $K(s)$ of a C sensor has the form:

$$K(s) = \frac{1}{s(R_r \cdot C) + 1} \qquad (17)$$

In this case we have obtained the following formula for $v_{out}(s)$ based on (2), (3), (6) and (17):

$$v_{out}(s) = V_{in} \cdot \left(\frac{1}{s} \cdot \frac{1}{s(R_r C) + 1} \right) \qquad (18)$$

which has the form in the time domain:

$$v_{out}(t) = V_{in} \cdot \left(1 - e^{\frac{-t}{R_r C}} \right) \text{ for } t \in (0; T) \qquad (19)$$

The ADC samples the signal $v_{out}(t)$ at a moment t_m as shown in Fig. 5. The voltage sample has the value $V_m = v_{out}(t_m)$. Transforming the formula (19) we have obtained the following formula for calculating the value C:

$$C = \frac{-t_m}{R_r \cdot \ln\left(1 - \frac{V_m}{V_{in}} \right)} \qquad (20)$$

Fig. 5 shows the timing of the measurement procedure for C measurements. When the voltage response v_{out} to a square pulse v_{in} increases to the threshold voltage level V_{cc_scaled} the AC simultaneously triggers the ADC and reading the current value from the timer (Fig. 2 and Fig. 3). Likewise, in this case, the measurement procedure duration is as short as possible, because $T = t_m + t_{ADC}$.

Also, for C measurements, we should determine the value V_{cc_scaled} and the value R_r for the best possible measurement accuracy of t_m and V_m.

Based on analyses of maximum relative measurement errors of voltage v_{out} described in Sections 3.1 and 3.3 it is proposed that the value V_{cc_scaled} should be chosen from within a voltage value range from 0.7 to 0.9 of the value V_{ref}.

As in the previous subsection, if we know the range of capacitance value changes (from C_{min} to C_{max}) of a C sensor and we have established the minimum value t_{m_min}, i.e. the number N_{min}, we can determine the minimum value R_{r_min} of R_r:

$$R_{r\_min} = \frac{-N_{min} \cdot T_{clk}}{C_{min} \cdot \ln\left(1 - \frac{V_{cc\_scale}}{V_{in}}\right)} \qquad (21)$$

Obviously, the greater the value R_r the greater the value t_m for a given value of C, what improves the accuracy of measurements of time t_m by the timer [32,33]. However, lengthening time t_m increases the energy consumption, what is disadvantageous, especially for battery-powered systems. The maximum value R_{r_max} of R_r is limited by the measurement range of the n-bit timer $t_{m\_max} = N_{max} \cdot T_{clk} \cdot P_{max}$, where $N_{max} = 2^n$, P_{max} – the maximum value of the prescaler of the timer. Hence, R_{r_max} can be calculated from:

$$R_{r\_\max} = \frac{-N_{\max} \cdot P_{\max} \cdot T_{clk}}{C_{max} \cdot \ln\left(1 - \frac{V_{cc\_scale}}{V_{in}}\right)} \qquad (22)$$

Finally, the value of R_r should be in a range from R_{r_min} to R_{r_max}, and this value should be a compromise between the measurement accuracy of measurements of time t_m and the energy consumed by the system during the measurement procedure.

3. Error analysis

The maximum possible relative inaccuracy (error) $\Delta f / |f|$ of an indirectly measurable variable f will be used to estimate the inaccuracy of determination of R, L and C values of the sensors from the measurement results. It is an approximation of the standard uncertainty [34] and has the form [35]:

$$\frac{\Delta f}{|f|} = \frac{1}{|f|} \cdot \sum_{i=1}^{I} \left|\frac{\partial f}{\partial x_i}\right| \cdot |\Delta x_i|, \qquad (23)$$

where: $f = f(x_1, x_2, .. , x_I) \neq 0$ – an indirectly measurable variable, $x_1, x_2, .. , x_I$ – directly measurable variables, Δf – the maximum absolute inaccuracy of the function f, Δx_i – the maximum absolute inaccuracy of a directly measurable variable x_i (i = 1, 2, .., I).

3.1. Estimation of measurement inaccuracy for R sensors

Basing on (7) and (23) the maximum possible relative inaccuracy $\Delta R_m / |R_m|$ of an indirectly measurable resistance $R_m = R_m(R_r, V_{in}, V_m)$ obtained the following form:

$$\frac{\Delta R_m}{R_m} = \frac{\Delta R_r}{R_r} + \frac{\Delta V_{in}}{V_{in} - V_m} + \frac{\Delta V_m}{V_{in} - V_m} \cdot \frac{V_{in}}{V_m}, \quad (24)$$

where: $R_m > 0$, $R_r > 0$, $V_{in} > 0$, $V_m > 0$ and $V_{in} > V_m$.

The first component of the formula (24) $\delta R_r = \Delta R_r / R_r$ can be interpreted as the tolerance of resistor R_r. Hence, we should decrease δR_r by the use of precision (high-precision) resistors. They have a tolerance of 0.1% (0.01%). If we need even more precision, we can use ultra-precision resistors with a tolerance of 0.005%. Another way can be to measure the resistance R_r with a precise multi-meter. E.g. the Agilent 34410A enables to measure resistance with accuracy of 0.0065% [36]. In this case, if we assume a 0.01% tolerance of R_r or we measure the value of R_r with a precise multi-meter, the value δR_r is small in comparison with the other components of the formula (24) and it can be omitted in the further analysis of $\Delta R_m / |R_m|$.

The second component $\delta V_{in\_R} = \Delta V_{in} / (V_{in} - V_m)$ represents the inaccuracy of determination of V_{in} value. This value is correlated with the supply voltage V_{CC} and thus with the reference voltage V_{ref}, because $V_{in} = Vcc - V_{Ron}$ and $V_{ref} = \xi \cdot Vcc$ ($\xi \leq 1$) or $V_{ref} = V_{CC} - V_D$ [28]. V_{Ron} is a voltage drop on the inverter's transistor (Fig. 3) [24]. The internal output resistance of the inverter that is a static drain-to-source on-resistance for N-channel for the IRF7015 (IRF7389) is equal to 0.16 Ω (0.046 Ω) at 4.5 V [37,38]. If we assume R_r = 2202 Ω, the voltage V_{Ron} is at most equal to 0.007% (0.002%) of the voltage V_{CC}, i.e. it is at most 0.29 (0.08) LSB for the 12-bit ADC resolution. Hence, we can assume that an inaccuracy of determination of V_{in} value is on a level of ±1 LSB (the quantisation error).

The greatest influence on the value of $\Delta R_m / |R_m|$ has the third component $\delta V_{m\_R} = \Delta V_m / (V_{in} - V_m) \cdot V_{in} / V_m$ of the formula (24). The absolute measurement inaccuracy ΔV_m of voltage V_m measured by the ADC depends on the measurement uncertainty ΔV_{ADC} of the ADC (±2 LSB for the ATXmega32A4) and noise (disturbances) Δv_{noise} generated by digital circuits of the microcontroller, inter alia by its core processor, timers and a clock system.

It should be mentioned that the impact of variations of the supply voltage V_{CC} on voltage measurements is negligible in comparison with δV_{in_R} and especially δV_{m_R}, because the formulas (7), and also (14) and (20) are functions of the ratio V_m/V_{in}. Thanks to this calculations of R, L and C values are theoretically independent of the reference voltage V_{ref} - that is also of the supply voltage

V_{cc} - and V_m and V_{in} are kept and used in calculations in the form of values corresponding to 12-bit codes read from the ADC

The graphs for δV_{in_R} and δV_{m_R} are shown in Fig. 6. It is seen that δV_{in_R} values for ±1 LSB of ΔV_{in} achieve 0.1% up to the end of ADC voltage range (Fig. 6a). Its values are in a range from 0.2% to 0.95% for ±10 LSB of ΔV_{in}, i.e. for a very inaccurate determination of V_{in} value.

The δV_{m_R} values are about ten times greater than the δV_{in_R} values. E.g. for the minimum value of ΔV_m equal to ±2 LSB (we take into account only the measurement uncertainty ΔV_{ADC} of the ADC) the δV_{m_R} values are following (Fig. 6b): 1.08% at the beginning, 0.16% at 2/3 and 0.24% at the end of the scale of the ADC. If we take into account the impact of disturbance Δv_{noise} on the measurement results of V_m (e.g. ΔV_m = ±10 LSB), the values of δV_{m_R} are respectively: 5.42%, 0.8% and 1.2%. Such large error values result from a small 12-bit resolution of the ADC built in the microcontroller. Because we are not able to influence the ΔV_{ADC} and Δv_{noise} values (they depend on a chosen microcontroller and its working conditions), we can minimize the inaccuracy δV_{m_R} only by selecting an appropriate value of resistor R_r, and more specifically by assuming the value ρ (10), so as the ADC does not have to measure too low voltage values (Fig. 6b).

3.2. Estimation of measurement inaccuracy for L sensors

To analyse the maximum possible relative inaccuracy $\Delta L / |L|$ of an indirectly measurable inductance L it is assumed that $R_r >> R_s$, i.e. $R_s \approx 0$. In this case the formula (14) becomes simpler:

$$L = \frac{-t_m \cdot R_r}{\ln\left(\frac{V_m}{V_{in}}\right)} \qquad (25)$$

and L is a function of $L(R_r, t_m, V_{in}, V_m)$. Hence, transforming (25) based on (23) we obtain the following formula for $\Delta L / |L|$:

$$\frac{\Delta L}{L} = \frac{\Delta R_r}{R_r} + \frac{\Delta t_m}{t_m} + \delta V_{in\_L} + \delta V_{m\_L} \qquad (26)$$

$$\delta V_{in\_L} = -\frac{\Delta V_{in}}{V_{in} \cdot \ln\left(\frac{V_m}{V_{in}}\right)} \quad \text{and} \quad \delta V_{m\_L} = -\frac{\Delta V_m}{V_m \cdot \ln\left(\frac{V_m}{V_{in}}\right)}, \qquad (27)$$

where: $L > 0$, $R_r > 0$, $t_m > 0$, $V_{in} > 0$, $V_m > 0$ and $V_{in} > V_m$.

Also in this case, the first component of the formula (26) $\delta R_r = \Delta R_r / R_r$ represents the tolerance of resistor R_r.

Because the time $t_m = N_m \cdot T_{clk}$, N_m – the number of pulses counted by the n-bit timer, the second component $\delta t_m = \Delta t_m / t_m$ depends on, generally speaking, the stability of the timer [32,33] $\Delta T_{clk} / T_{clk}$ and the quantisation error $1 / N_m$, which for small values of N_m has a significant share in the inaccuracy $\Delta L / |L|$. Due to the way of controlling the timer trigger noise does not affect the accuracy of determining the time t_m.

The graphs for two last components of (26) δV_{in_L} and δV_{m_L} are shown in Fig. 7. They have the same shapes and values for given V_m and $\Delta V = \Delta V_{in} = \Delta V_m$, what follows from (27). Hence, the δV_{in_L} values for ±1 LSB of ΔV_{in} do not exceed a level of 0.16% and they reach the minimum 0.06% in the middle of the ADC range. For ±2 LSB of ΔV_m we obtained two times, and for ±10 LSB of ΔV_m - ten times greater values of δV_{m_L} than for ±1 LSB (27).

From Fig. 7 it is seen that the minimum values of δV_{in_L} and δV_{m_L} are in the middle of the ADC range, therefore a threshold voltage level value V_{cc_scaled} should be set to this value, i.e., if we take into account the resistance R_s, to the middle value of the range of observable changes of voltage v_{out} (16).

3.3. Estimation of measurement inaccuracy for C sensors

In this case the formula for the maximum possible relative inaccuracy $\Delta C / |C|$ of an indirectly measurable capacitance $C = C(R_r, t_m, V_{in}, V_m)$ is derived from (20) based on (24) and has the form:

$$\frac{\Delta C}{C} = \frac{\Delta R_r}{R_r} + \frac{\Delta t_m}{t_m} + \delta V_{in\_C} + \delta V_{m\_C} \qquad (28)$$

$$\delta V_{in\_C} = \frac{V_m \cdot \Delta V_{in}}{V_{in} \cdot (V_{in} - V_m) \cdot \ln\left(1 - \frac{V_m}{V_{in}}\right)} \quad \text{and} \quad \delta V_{m\_C} = \frac{\Delta V_m}{(V_{in} - V_m) \cdot \ln\left(1 - \frac{V_m}{V_{in}}\right)}, \qquad (29)$$

where: $C > 0$, $R_r > 0$, $t_m > 0$, $V_{in} > 0$, $V_m > 0$ and $V_{in} > V_m$.

The first and second components of the formula (28) have already been explained when discussing the formulas (24) and (26), whereas two last components δV_{in_C} and δV_{m_C} in functions of V_m and ΔV_{in} or ΔV_m , respectively, are plotted in Fig. 8.

It is seen in Fig. 8 that the values of δV_{in_C} for ±1 LSB (±10 LSB) of ΔV_{in} increase from 0.02% (0.2%) to 0.05% (0.5%), whereas the values of δV_{m_C} for ±2 LSB (±10 LSB) of ΔV_m decrease from 1.06% (5.3%) to 0.12% (0.6%) for increasing values of V_m.

To establish the threshold voltage level value V_{cc_scaled} there was determined the value $V_{m\_min} = 0.66 \cdot V_{ref}$ of voltage V_m for which the sum δV_{sum_C} of δV_{in_C} for ±1 LSB and δV_{m_C} for

±2 LSB is minimal and equal to 0.143%. The V_{m_min} value was set in the 6-bit V_{CC} voltage scaler of AD. Due to non-linearity of the voltage scaler [28] it turned out from the measurements (described in Subsection 4.3) that V_{cc_scaled} is equal to $0.82 \cdot V_{ref}$. Despite this, this value was left, because the sum δV_{sum_C} increased only by 0.003%, i.e. practically it has no influence on the value of $\Delta C / | C |$.

4. Experimental results and discussion

The experiments were performed by using a prototype board of the laboratory compact smart sensor, consisted of a microcontroller module (the ATXmega32A4 together with a 16 MHz crystal oscillator), an inverter based on IRF7015, a communication module MMusb232 based on FT232BL and a sensor interface circuit.

An Agilent 34410A Digital Multimeter was used to measure the supply voltage (V_{CC} = 3.301 V) and values of reference resistors (R_r = 2202 Ω for R measurements, R_r = 10 Ω for L measurements, R_r = 471 Ω for C measurements). Also, the reference voltage value was determined (V_{ref} = 2.615 V).

Preliminary experimental studies have shown that the ADC is characterized by large offset and gain errors, making it practically useless for small voltage values. Therefore, scaling of the ADC was performed. On this purpose, an Agilent E3631A as the source of reference voltage was used. The results were used to the run-time compensation based on integer arithmetic calculations of the offset and gain errors of the ADC by the software. The compensation (error correction) is based on the simple formula:

$$v_{ac} = v_{bc} - \xi \cdot \left(\frac{2^n - v_{bc}}{2^n} \right) \square \square \square, \qquad (30)$$

where: n – ADC resolution, v_{bc} – a voltage before correction directly measured by the ADC, v_{ac} – a voltage after software correction, ξ = 202 – a value of the coefficient determined from measurement results for the 12-bit ADC of ATXmega32A4.

The voltage measurement results of the ADC before and after correction are shown in Fig. 9, and relative measurement errors - in Fig. 10. It is seen in Fig. 10 that the error correction enables to reduce by over one hundred times the ADC errors for small voltage values, thus making the errors less than 0.7%.

4.1. Measurements for R sensors

The measurements for the R sensor configuration of the direct sensor-to-microcontroller interface were carried out for 24 resistance values of R_m resistor: from 100 Ω to 8200 Ω, according

to the standard values of E12 series. There was used a decade MDR-93-6a resistor to set individual resistance values R_x of R_m. The ADC sampled the voltage response V_{out} four times; after that the result was averaged. The measurement results of voltages V_m and values of R_m calculated by the microcontroller were sent to a personal computer via a USB interface. The measurements for a given value of R_m were repeated several dozens of times (at least 64 times). Each time, the lowest, middle, and highest values from the set of measurement results were selected and saved. The lowest and highest values are plotted in the form of points, whereas middle values were used to plot the curves presented in Fig. 11 and Fig. 12.

The results of scaling of the direct interface for voltages (Fig. 11a) and resistances (Fig. 11b) are shown in Fig. 11, where R_x represents reference resistor values set by the decade resistor. The relative errors of resistance determination are drawn in Fig. 12, whereas the errors of resistance values calculated directly from measurement results are given in Fig. 12a, and the errors of resistance values after software correction - in Fig. 12b. The vertical lines join points representing the maximum and minimum values of the errors, i.e. they represent the maximum uncertainty of resistance determination.

Analysing Fig. 11a we can observe that the graph of relative errors is a function, what additionally was confirmed by dozens of measurements. Hence, it is possible to minimize this error by the software. For this purpose, a piecewise linear function (PLF) composed of three linear segments approximating the error function is defined. There were used only three segments, which ensures an optimum fit with the simplest possible calculation. Thus, the PLF is described by the following coefficients: a_i, b_i for $R_{i-1} < R_m \leq R_i$, where i = 1, 2, 3, and $R_0 = 0$, R_i – threshold values of resistance for individual segments of PLF. Then, a new corrected value R_{m_corr} is calculated in the following way: $R_{m\_corr} = R_m - b_i - a_i \cdot R_m$.

Thanks to this simple operation we have obtained a two-fold reduction of the relative error for small values of R_m - to a level less than 3% (Fig. 12b). As it is seen in Fig. 12b, the smallest errors are for values of R_m similar to the value of R_r (0.6%) and they grow to 1.2% at the end of the measuring range of resistances, which is consistent with the theoretical considerations (Fig. 6). These values of relative errors (Fig. 12b) correspond to the values of the maximum relative inaccuracy determined for ±5 LSB (Fig. 6). Hence, we can notice that noise increases the absolute measurement inaccuracy ΔV_m by about ±3 LSB (the minimum value of $\Delta V_m = \Delta V_{ADC}$ = ±2 LSB).

Obviously, to minimize the impact of noise we can add to the direct R sensor-to-microcontroller interface circuit – in parallel to R - a capacitor suppressing interferences, but we should remember that this solution extends the measurement time [25].

4.2. Measurements for L sensors

The measurements and processing the measurement data for an L sensor were carried out in accordance with the procedure described in the previous subsection. In this case, a set of measuring coils CPQL – 6 was used to determine individual inductance values of L. Before these measurements the inductance L_x and serial resistance R_s values of the measuring coils were measured by the Agilent 4263B LCR meter at 1 kHz. All measurement results are presented in Table 1, where L_x * – the value measured by the Agilent 4263B, L – the value calculated by the microcontroller based on the values: R_s, t_m and V_m.

Table 1. The measurement results for the direct L sensor -to-microcontroller interface circuit

L_x (L_x *) [mH]	R_s [Ω]	t_m [*0.0625 μs] min, middle, max	V_m [*657 μs] min, middle, max	L [μH] min, middle, max
0.1 (0.09843)	0.3412	105, 105, 105	2567, 2569, 2570	96.6, 96.7, 96.8
0.3 (0.3003)	0.5085	231, 231, 231	3096, 3098, 3099	294.7, 295.1, 295.3
1 (1.0157)	1.0157	699, 699, 699	3299, 3301, 3302	993.4, 995.0, 995.7
3 (2.9954)	3.201	2013, 2013, 2013	3362, 3363, 3364	2912.7, 2915.1, 2917.4
10 (10.025)	6.082	7135, 7135, 7137	3386, 3387, 3388	9722.9, 9731.8, 9743.4
30 (29.759)	7.001	21193, 21193, 21198	3391, 3393, 3394	28212.8, 28266.1, 28299.5

The measurement results from Table 1 are illustrated in Fig. 13. From Table 1 (the third column) and Fig. 13c it is seen that the AC works correctly and triggers both the reading from the timer and the ADC whenever the threshold voltage V_{cc_scaled} value is constant.

The shape of the graph in Fig. 13b, the fact that V_m is not constant, follows from two facts. The reading from the timer and the ADC are triggered by the AC with a short and constant time delay due to the time required by the AC interrupt service. Therefore, the smaller the inductance value of L, the greater the voltage drop of v_{out} (Fig. 4) at the same time, i.e. the lower voltage value measured by the ADC. However, this fact does not influence the final results because the ADC and the reading from the timer are triggered simultaneously. The second reason is undercharging of the sample and hold circuit of the ADC. This circuit is designed in such a way as to provide a given resolution at a given conversion speed, i.e. at a given sampling time, but for DC voltages [28,39]. Hence, for small values of L the voltage measurement results are underestimated.

The relative errors of inductance determination before and after software correction are drawn in Fig. 12. In this case also the three-segment PLF was used. Thanks to this, the obtained relative errors were less than 0.3%, and in some cases less than 0.1% (Fig. 12b), what is a very good result. These values of relative errors correspond to the maximum relative inaccuracy values drawn in Fig.

7 for $\Delta V_m = \Delta V_{ADC} = \pm 2$ LSB. Such a small value of ΔV_m is due to the fact that the L sensor interface circuit (a serial connection of R_r, R_s and L) works as a low-pass filter which filters noise (disturbances) at the ADC input, what is an important advantage improving the measurement accuracy.

4.3. Measurements for C sensors

For a C sensor the measurements were carried out for 26 capacitance values of a C capacitor: from 100 nF to 12000 nF, also according to the standard values of E12 series. Individual capacitance values C_x of C were set up to 1000 nF using a decade condenser TYPE DK5. For setting values exceeding 1000 nF a decade condenser TYPE DK50 was used. The capacitance values set in decades were verified by a 4263B LCR meter at 1 kHz frequency.

Also in this case, the measurements and processing the measurement data including software correction were carried out in accordance with the procedures described in the previous subsections. These results are depicted in Fig. 15 (scaling of the C sensor interface) and in Fig. 16 (the relative errors of capacitance determination before and after software correction).

It is seen in Fig. 15b that V_m is also not constant. This is due to the fact that the smaller the capacitance value of C, the higher the voltage value measured by the ADC. It follows from the fact that for small capacitance values the voltage growth of v_{out} (Fig. 5) at the same time is greater, inversely to that of the inductance (i.e. for small values of C the voltage measurement results are overestimated).

There were obtained the relative errors of capacitance determination after software correction at a level of 0.2% (Fig. 16b), what is also a very good result. It corresponds to the maximum relative inaccuracy values drawn in Fig. 8 also for $\Delta V_m = \Delta V_{ADC} = \pm 2$ LSB. Hence, the C sensor interface circuit (a serial connection of R_r and C) is a low-pass filter likewise filtering noise at the ADC input.

5. Comparison of the methods with the state of the art

The results of comparison of the proposed methods based on a versatile direct sensor-to-microcontroller interface circuit (VDSMIC) with the state of the art, that is with the 1-, 2- and 3-point (generally n-point) calibration technique methods (n-PCT) based on the direct sensor-to-microcontroller interface circuits are included in Table 2. In this table there are compared the interface circuit complexity and the maximum measurement relative error for R, L and C measurements. For R measurements the proposed VDSMIC methods are compared with the 1-, 2-

and 3-point methods presented in [9], for L measurements - with the 1-point method described in [17] and for C measurements - with the 3-point method proposed in [18].

Table 2. Comparison of the proposed methods with the n-point calibration technique methods based on the direct sensor-to-microcontroller interface circuits

	Interface circuit		*Max. relative error*	
Method / Measured component	*VDSMIC*	***n*-PCT**	*VDSMIC*	***n*-PCT**
R_x	$\boldsymbol{R_r}$	1- R_{c1}, C 2- R_{c1}, R_{c2}, C 3- R_{c2}, R_0, C	**1%** (1)	0.55% (1) 0.016% (1) 0.01% (1)
L_x		1- R_0, L_r	**0.3%** (2)	0.45% (3) 1.98% (4)
C_x		3- R_d, R_i, C_c, (C_{off})	**0.2%** (5)	0.036% (6)

Notes:

(1) for the range of R_x from 825 Ω to 1470 Ω,

(2) for the range of L_x from 0.1 mH to 30 mH,

(3) for the range of L_x from 1 mH to 10 mH,

(4) for the range of L_x from 10 mH to 100 mH,

(5) for the range of C_x from 100 nF to 12 μF,

(6) for the range of C_x from 149 pF to 206 pF.

It is seen from Table 2 that the main advantage of the proposed approach is simplicity and versatility of the interface circuit. In all cases we use only one component – the reference resistor R_r, instead of one or two reference resistors and one capacitor for R and C measurements and instead of one resistor limiting the current and one reference inductor for L measurements. This advantage may be especially important for L measurements, because we don't need an uncomfortable element which is the reference inductor – often it has large dimensions and a big tolerance, e.g. 10%.

Unfortunately, the formulas (14) and (20) used to compute the L and C sensor values involve a natural log function. The code of this function was optimised. For this reason calculation of (14) by the 8-bit microcontroller with a 16 MHz external clock takes 1000 μs, and (20) - 950 μs, what is relatively short for such microcontrollers and thus can be acceptable.

It is worth mentioning that for *R* measurements the measurement procedure is definitely shorter (about one hundred times) and consumes less energy (also about one hundred times) in comparison with the 1-point calibration technique method, but it is burdened with a large measurement error. Therefore, the chosen method should depend on the application requirements (the measurement speed and the low energy consumption or the measurement accuracy).

6. Conclusions

In the paper new time-domain measurement methods for determining values of *R*, *L* and *C* sensors based on a direct sensor-to-microcontroller interface circuit for microcontrollers with internal ADCs and ACs are presented. These methods use only one common hardware configuration of the interface circuit consisting of a reference resistor, a given sensor, an inverter and a microcontroller. However, the measurement procedures and ways of determining the values for a given *R*, *L* or *C* sensor implemented in the microcontroller software differ from each other.

A prototype of the proposed complete application of a compact smart sensor based on the ATXmega32A4 microcontroller has been developed and tested. The experimental results are compatible with the theoretical ones. There were achieved the following relative errors of value determination: for an *R* sensor - less than 3%, for an *L* sensor - less than 0.3%, and for a *C* sensor - less than 0.2%, for the 12-bit ADC. Such very good results for *L* and *C* sensors result from the fact that they together with the reference resistor form low-pass filters which filter disturbances at the ADC input.

It should be emphasized that the proposed solution of the sensor interface is a simple and versatile; the measurement procedures based on the new time-domain methods are short and thus low-cost and low-power ones. Also, the determination of sensor values is not complicated - thanks to this the software implementing these methods needs a little space in program and data memories (codes of the measurement functions occupy 486 B, and codes of the correction and calculation functions take 2252 B – written in the C language and compiled by the AVR GCC in the Atmel Studio 6).

Therefore, we can design smart sensors based on the proposed solution even for 8-bit microcontrollers, what is presented in the paper. Its greatest advantage is that we can use it to extend the functionality of the existing microcontroller systems by direct sensor-to-microcontroller interface circuits in a simple and cheap way.

References

[1] G. Tuna, V. C . Gungor, Ch2 – Energy harvesting and battery technologies for powering wireless sensor networks, Industrial Wireless Sensor Networks. Woodhead Publishing (2016), 25-38.

[2] M. Kuorilehto, M. Kohvakka, J. Suhonen, P. Hamalainen, M. Hannikainen T. D. Hamalainen, Ultra-low energy wireless sensor networks in practice, John Wiley & Sons, Ltd., Great Britain, 2007.

[3] J. Hoja, G. Lentka, Interface circuit for impedance sensors using two specialized single-chip microsystems, Sensors and Actuators A 163 (2010) 191–197.

[4] C. Falconi, E. Martinelli, C. Di Natale, A. D'Amico, F. Maloberti, P. Malcovati, A. Baschirotto, V. Stornelli, G. Ferri, Electronic interfaces, Sensors and Actuators B 121 (2007) 295–329.

[5] Microchip Technology, PT100 RTD Evaluation Board User's Guide, (2007), Available at: http://ww1.microchip.com/downloads /en/DeviceDoc/51607b.pdf.

[6] Maxim Integrated Products Inc., Positive Analog Feedback Compensates PT100 Transducer, (2005), Available at: *http://www.maximintegrated.com/en/app-notes/index.mvp/id/3450*.

[7] Texas Instruments, AN-1559 Practical RTD Interface Solutions, (2013), Available at: http://www.ti.com/lit/an/snoa481b/snoa481b.pdf.

[8] E. Sifuentes, R. Gonzalez-Landaeta, J. Cota-Ruiz, F. Reverter, Measuring dynamic signals with direct sensor-to-microcontroller interfaces applied to a magnetoresistive sensor, Sensors 17, 1150 (2017) doi:10.3390/s17051150.

[9] F. Reverter, J. Jordana, M. Gasulla, R. Pallàs-Areny, Accuracy and resolution of direct resistive sensor-to-microcontroller interfaces, Sensors and Actuators A 121 (2005) 78–87.

[10] L. Bengtsson, Direct analog-to-microcontroller interfacing, Sensors and Actuators A 179 (2012) 105– 113.

[11] F. Reverter, M. Gasulla, R. Pallàs-Areny, Analysis of power-supply interference effects on direct sensor-to-microcontroller interfaces, IEEE Transactions on Instrumentation and Measurement 56 (1) (2007) 171-177.

[12] F. Reverter, The Art of Directly Interfacing Sensors to Microcontrollers, Journal of Low Power Electronics and Applications (2) (2012) 265-281.

[13] L. Bengtsson, Analysis of direct sensor-to-embedded systems interfacing: a comparison of targets' performance, International Journal of Intelligent Mechatronics and Robotics 2 (1) (2012) 41-56.

[14] F. Reverter, Ò. Casas, Interfacing differential resistive sensors to microcontrollers: A direct approach, IEEE Transactions on Instrumentation and Measurement 58 (10) (2009) 3405-3410.

[15] E. Sifuentes, O. Casas, F. Reverter, R. Pallàs-Areny, Direct interface circuit to linearise resistive sensor bridges, Sensors and Actuators A 147 (2008) 210–215.

[16] J. Jordana, R. Pallàs-Areny, A simple, efficient interface circuit for piezoresistive pressure sensors, Sensors and Actuators A 127 (2006) 69–73.

[17] Z. Kokolanskia, J. Jordanab, M. Gasullab, V. Dimceva, F. Reverterb, Direct inductive sensor-to-microcontroller interface circuit, Sensors and Actuators A 224 (2015) 185–191.

[18] F. Reverter, O. Casas, Direct interface circuit for capacitive humidity sensors, Sensors and Actuators A 143 (2008) 315–322.

[19] F. Reverter, O. Casas, A microcontroller-based interface circuit for lossy capacitive sensors, Measurement Science Technology 21 (2010) 065203, 1-8.

[20] F. Reverter, O. Casas, Interfacing Differential Capacitive Sensors to Microcontrollers: A Direct Approach, IEEE Transactions on Instrumentation and Measurement 59 (2010) 2763-2769.

[21] Z. Kokolanski, C. Gavrovski, V. Dimcev, Modified single point calibration with improved accuracy in direct sensor-to-microcontroller interface, Measurement 53 (2014) 22–29.

[22] Z. Kokolanski, C. Gavrovski, V. Dimcev, M. Makraduli, Hardware techniques for improving the calibration performance of direct resistive sensor-to-microcontroller interface, Metrology and Measurement System, XX (4) (2013) 529–542.

[23] Z. Kokolanski, F. Reverter, C. Gavrovski, V. Dimcev, Improving the resolution in direct inductive sensor-to-microcontroller interface, Annual Journal Of Electronics (2015) 135-138.

[24] Z. Czaja, A microcontroller system for measurement of three independent components in impedance sensors using a single square pulse, Sensors and Actuators A 173 (2012) 284-292.

[25] Z. Czaja, An implementation of a compact smart resistive sensor based on a microcontroller with an internal ADC, Metrology and Measurement Systems 23 (2016) 255-238.

[26] Z. Czaja, A method of measuring RLC components for microcontroller systems, Przegląd Elektrotechniczny (Electrical Review) 93 (2017) 37-40.

[27] International Rectifier, IRF7105 HEXFET Power MOSFET, (2003), Available at: http://www.irf.com/product-info/datasheets/data/irf7105.pdf.

[28] Atmel Corporation, 8-bit XMEGA A Microcontroller, XMEGA AU MANUAL, (2013), Available at: http://www.atmel.com/images/atmel-8331-8-and-16-bit-avr-microcontroller-xmega-au_manual.pdf.

[29] J. Watkinson, The art of digital audio, Third Edition, Elsevier (2001).

[30] International Standard, IEC 60751:2008, Industrial platinum resistance thermometers and platinum temperature sensors, 2.0 edn., International Electrotechnical Commission, Geneva, Switzerland, (2008).

[31] E.G. Bakhoum, M.H.M. Cheng, High-sensitivity inductive pressure sensor, IEEE Transactions on Instrumentation and Measurement 60 (2011) 2960-2966.

[32] F. Reverter, R. Pall`as-Areny, Effective number of resolution bits in direct sensor-to-microcontroller interfaces, Measurement Science and Technology 15 (2004) 2157–2162.

[33] F. Reverter, R. Pallàs-Areny, Uncertainty reduction techniques in microcontroller-based time measurements, Sensors and Actuators A 127 (2006) 74–79.

[34] I. Farrance, R. Frenkel, Uncertainty of measurement: A review of the rules for calculating uncertainty components through functional relationships, The Clinical Biochemist Reviews 33 (2012), 49-75.

[35] K. Kolikov, G. Krastevy, Y. Epitropov, A. Corlat, Analytically determining of the relative inaccuracy (error) of indirectly measurable variable and dimensionless scale characterizing quality of the experiment, Computer Science Journal of Moldova 20 (58) (2012) 15-32.

[36] Agilent Technologies, Agilent 34410A/11A 6 1/2 digit multimeter user's guide (2012).

[37] International Rectifier, IRF7105 HEXFET Power MOSFET, (2003), Available at: http://www.infineon.com/dgdl/irf7105.pdf.

[38] International Rectifier, IRF7389PbF HEXFET Power MOSFET, (2004), Available at: http://www.infineon.com/dgdl/irf7389pbf.pdf.

[39] Atmel Corporation, Atmel AVR1300: Using the Atmel AVR XMEGA ADC, (2013), Available at: http://www.atmel.com/images/atmel-8032-using-the-atmel-avr-xmega-adc_application-note_avr1300.pdf.

Figures captions

Fig.1. An example of a smart microcontroller sensor with a direct sensor-to-microcontroller interface circuit.

Fig. 2. Proposed direct sensor-to-microcontroller interface circuit for *R*, *L* and *C* sensors.

Fig. 3. Block scheme of the compact smart sensor for *R*, *L* and *C* sensors based on the ATxmega32A4 microcontroller.

Fig. 4. Voltage waveforms at the microcontroller pins during the measurement procedure for the *L* sensor (L = 1 mH, R_s = 1.987 Ω, R_r = 10 Ω).

Fig. 5. Voltage waveforms at the microcontroller pins during the measurement procedure for the *C* sensor (C = 1.0186 μF, R_r = 471 Ω).

Fig. 6. Graphs of the inaccuracy of determination of: (a) the value of V_{in}, (a) the value of V_m, for the *R* sensor.

Fig. 7. Graphs of the inaccuracy of determination of the value of V_{in} and the value of V_m, for the *L* sensor.

Fig. 8. Graphs of the inaccuracy of determination of: (a) the value of V_{in}, (a) the value of V_m, for the *C* sensor.

Fig. 9. Scaling of the 12-bit ADC of the ATxmega32A4 microcontroller.

Fig. 10. Relative errors of the scaling of the ADC: (a) before software correction, (b) after software correction.

Fig. 11. (a) Scaling of the *R* sensor. (b) Graph of V_m in a function of R_x for the *R* sensor.

Fig. 12. Relative errors of the resistance value determination for the *R* sensor: (a) before software correction, (b) after software correction.

Fig. 13. (a) Scaling of the *L* sensor. (b) Graph of V_m in a function of L_x for the *L* sensor. (c) Graph of t_m in a function of L_x for the *L* sensor.

Fig. 14. Relative errors of the inductance value determination for the *L* sensor: (a) before software correction, (b) after software correction.

Fig. 15. (a) Scaling of the *C* sensor. (b) Graph of V_m in a function of C_x for the *C* sensor. (c) Graph of t_m in a function of C_x for the *C* sensor.

Fig. 16. Relative errors of the capacitance value determination for the *C* sensor: (a) before software correction, (b) after software correction.

Figure 1

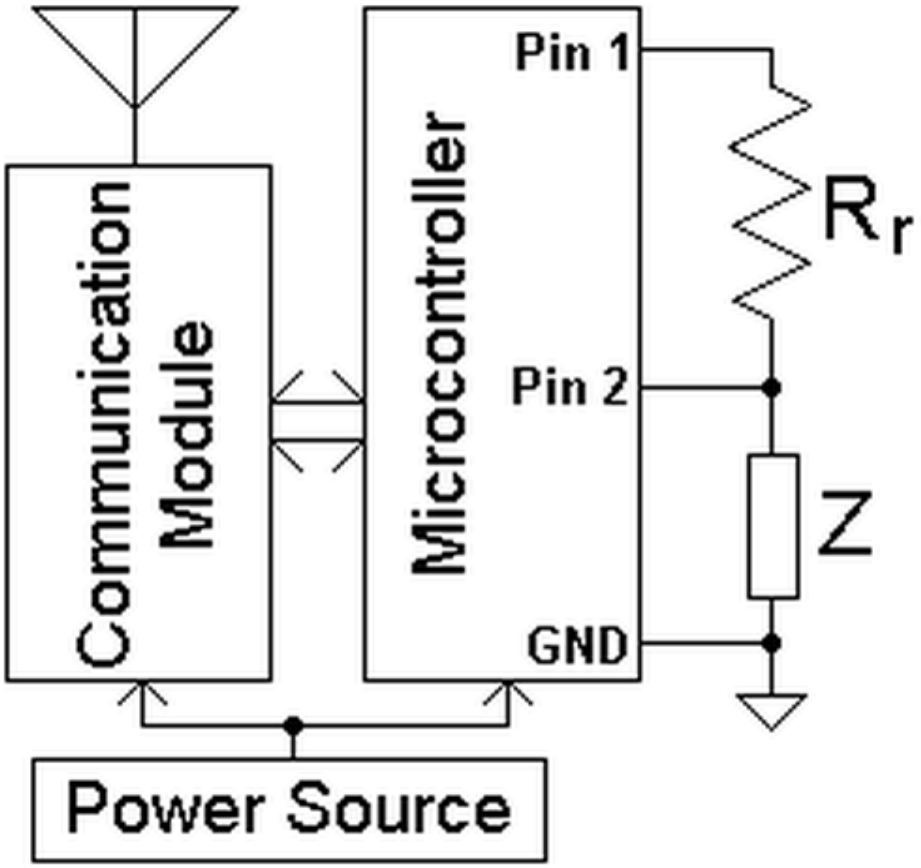

Figure 2

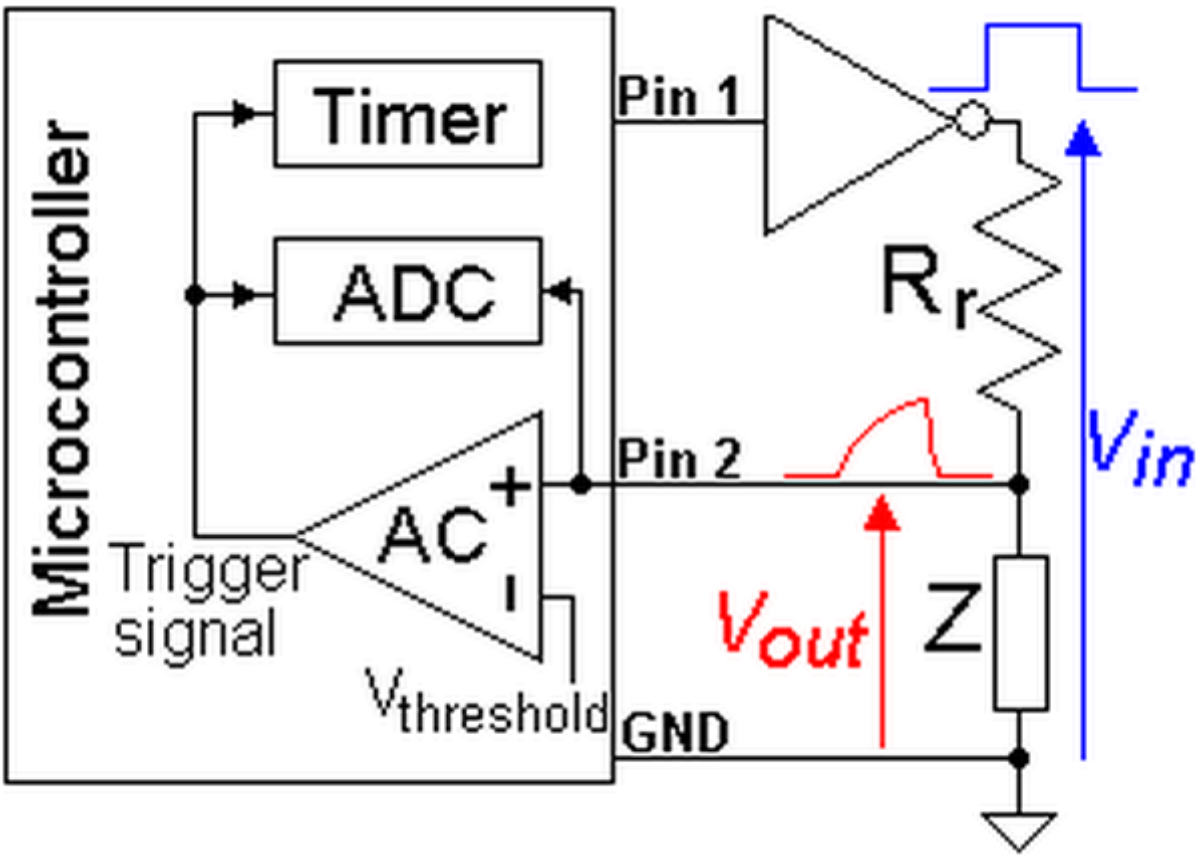

Figure 3

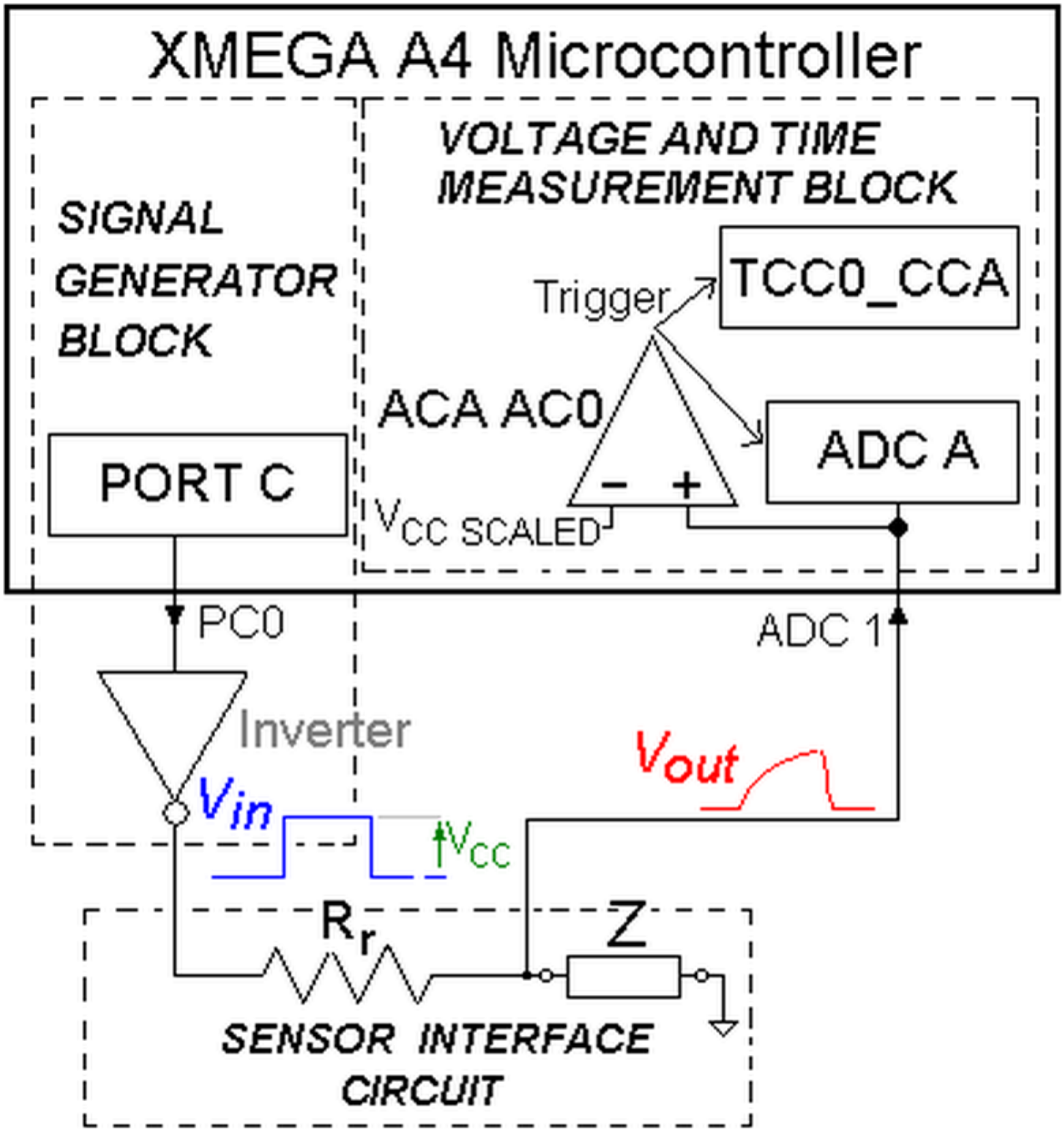

Figure 4

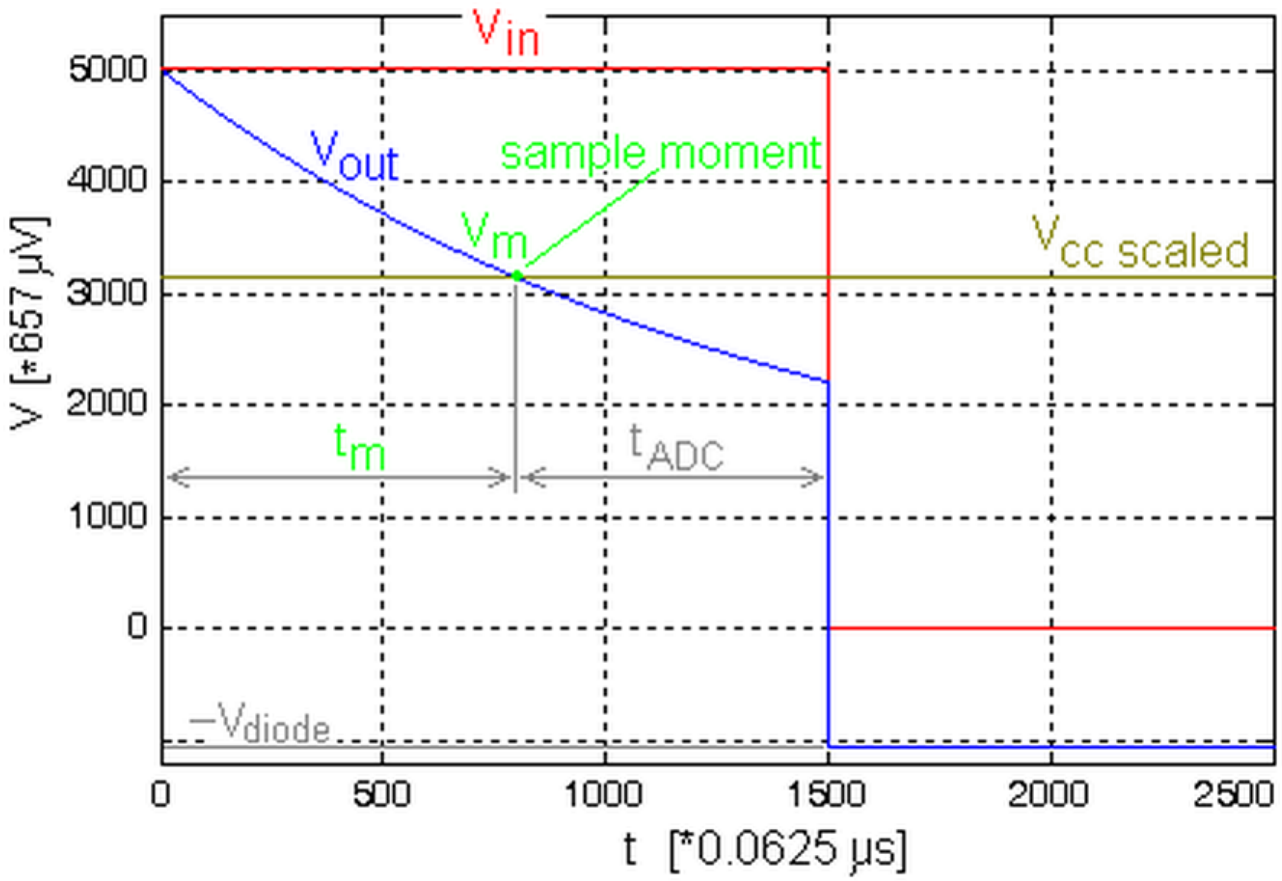

Figure 5

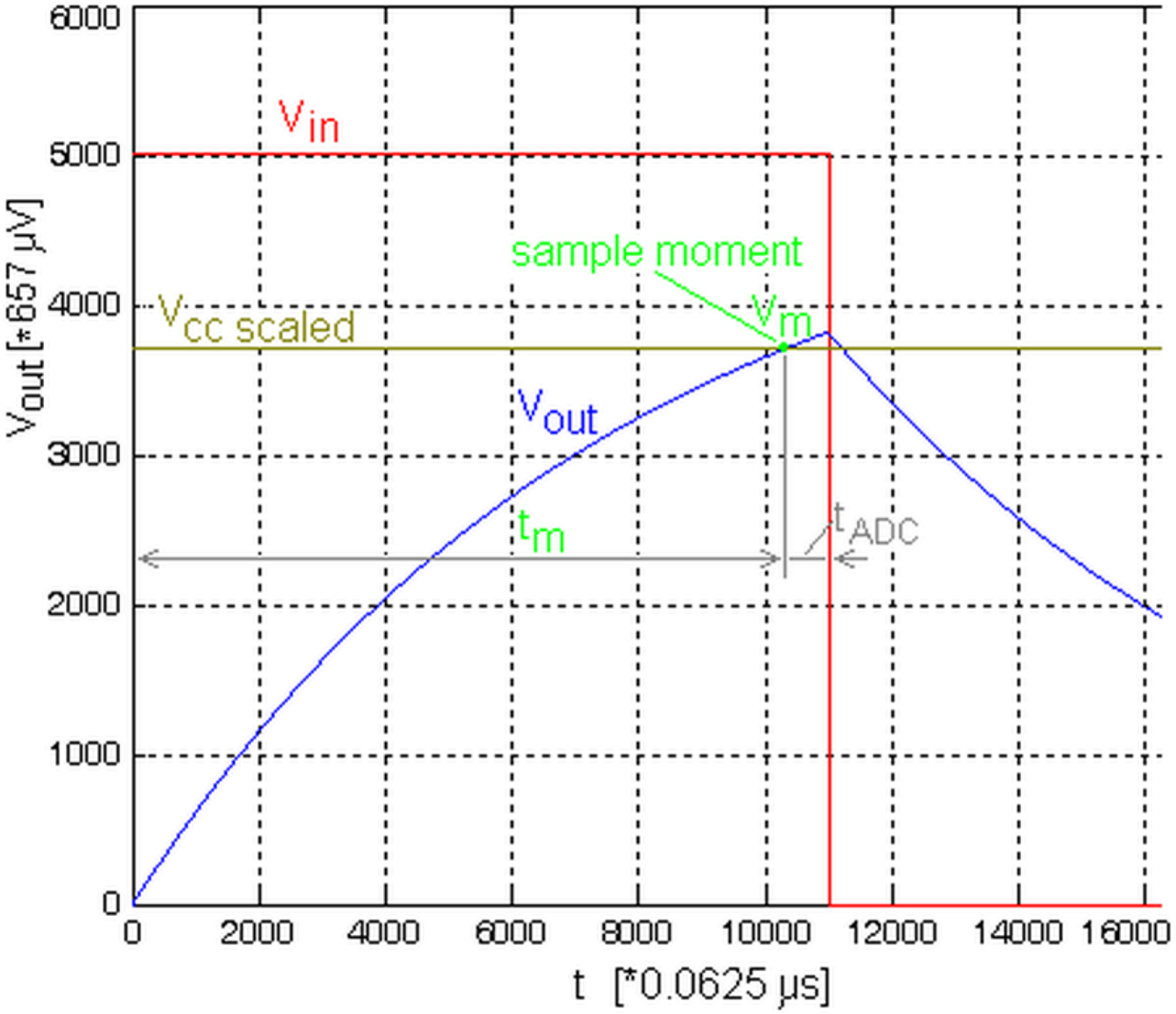

Figure 6

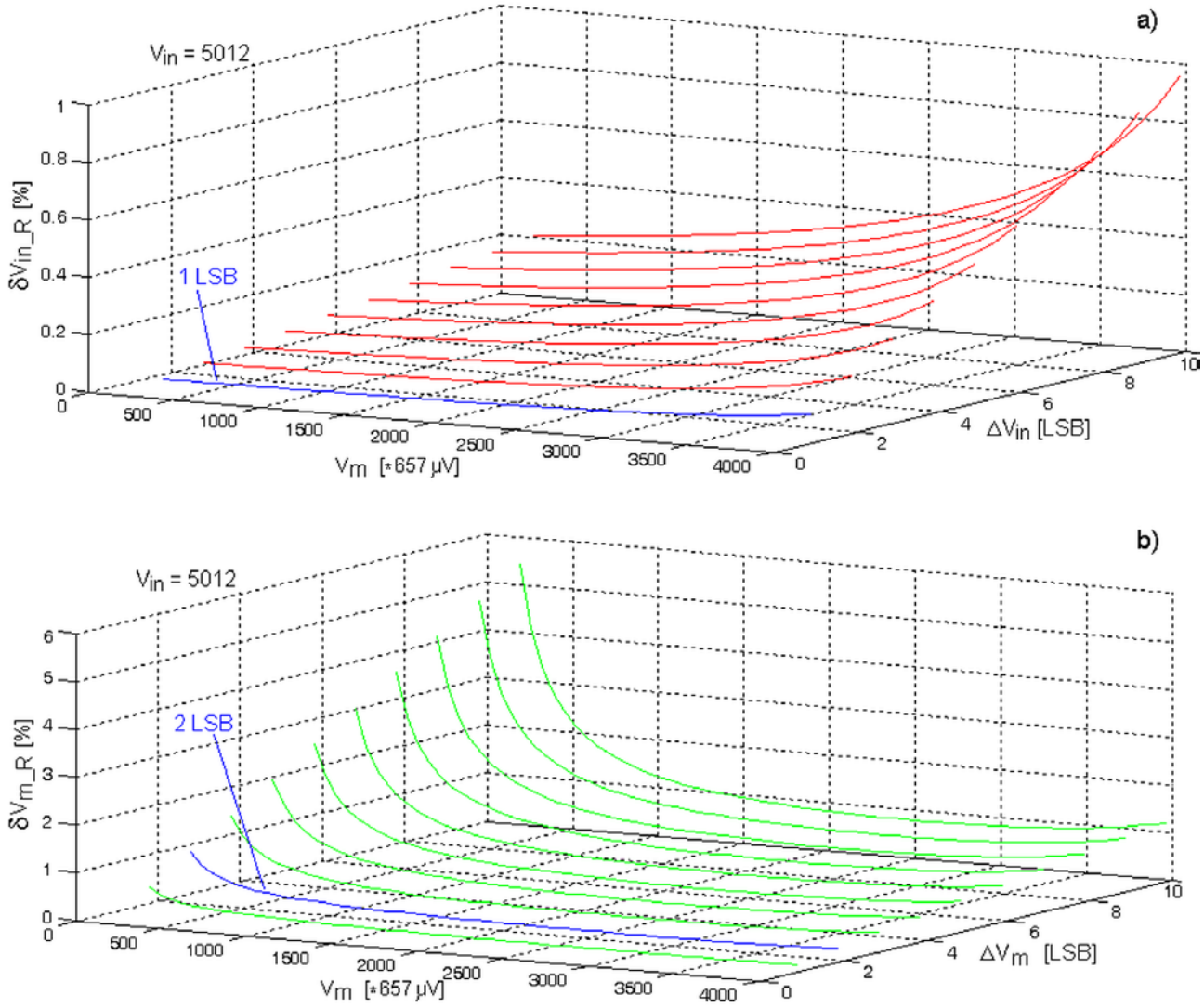

Figure 7

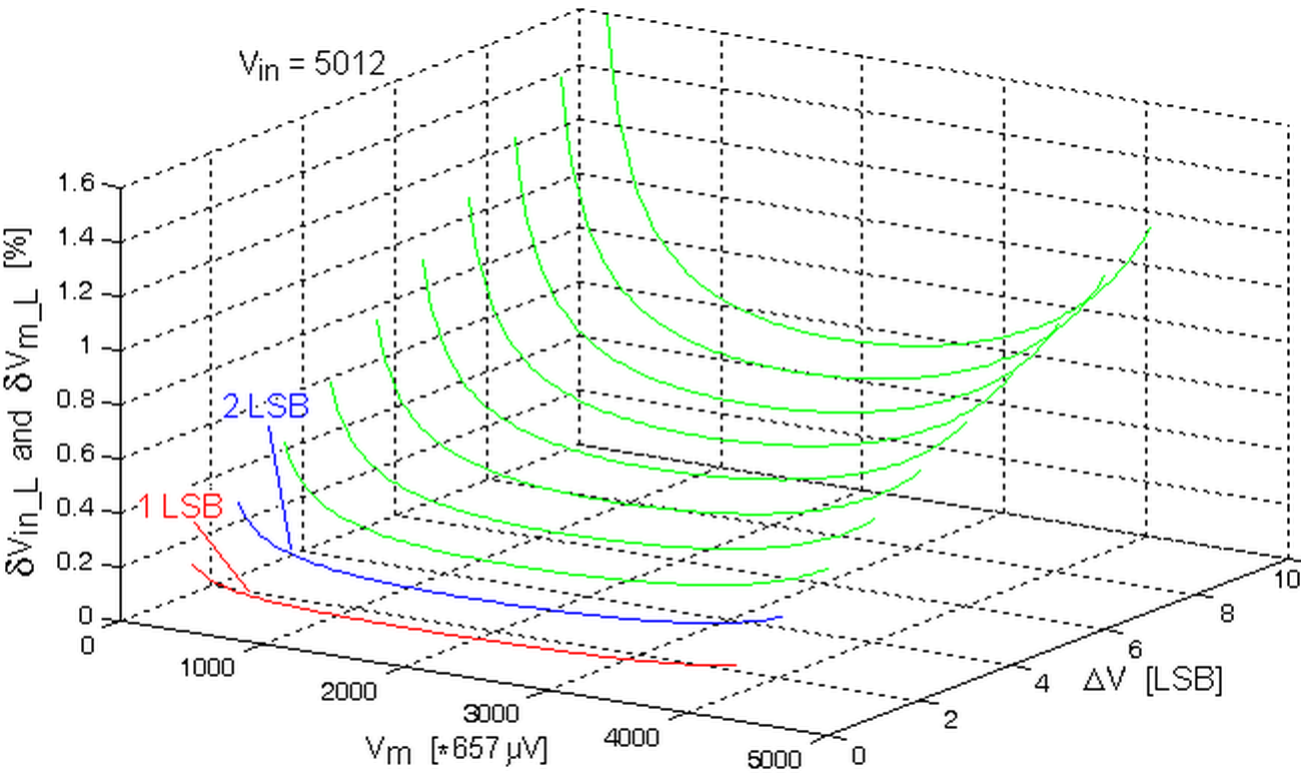

Figure 8

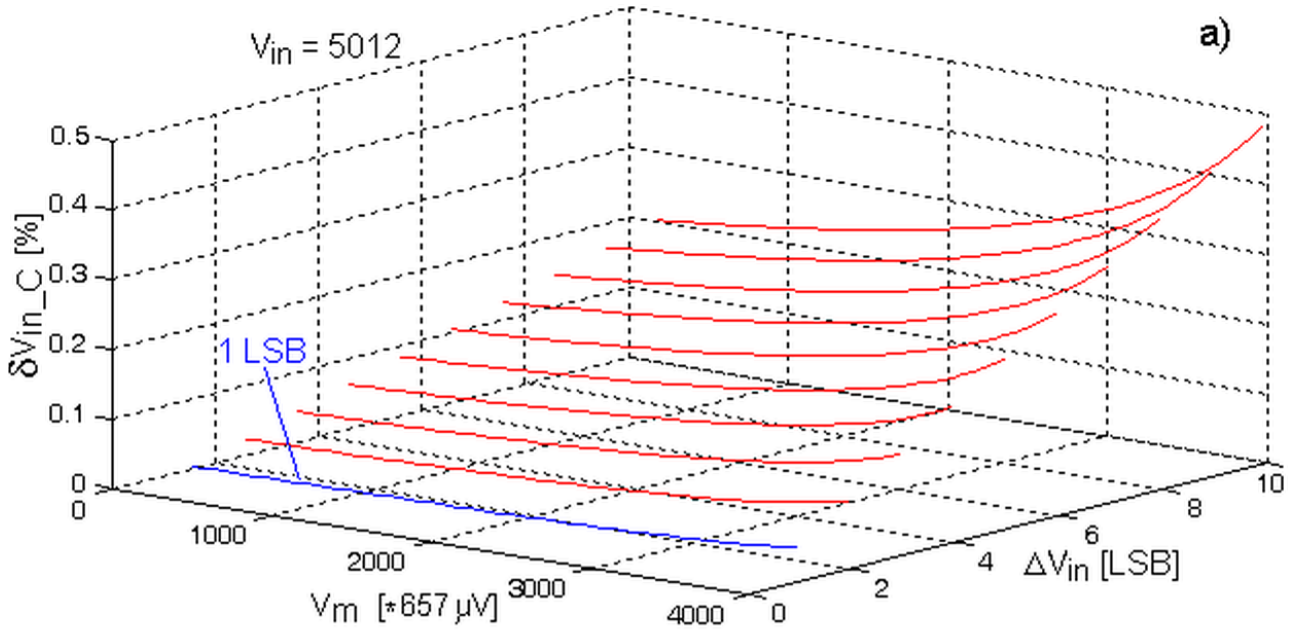

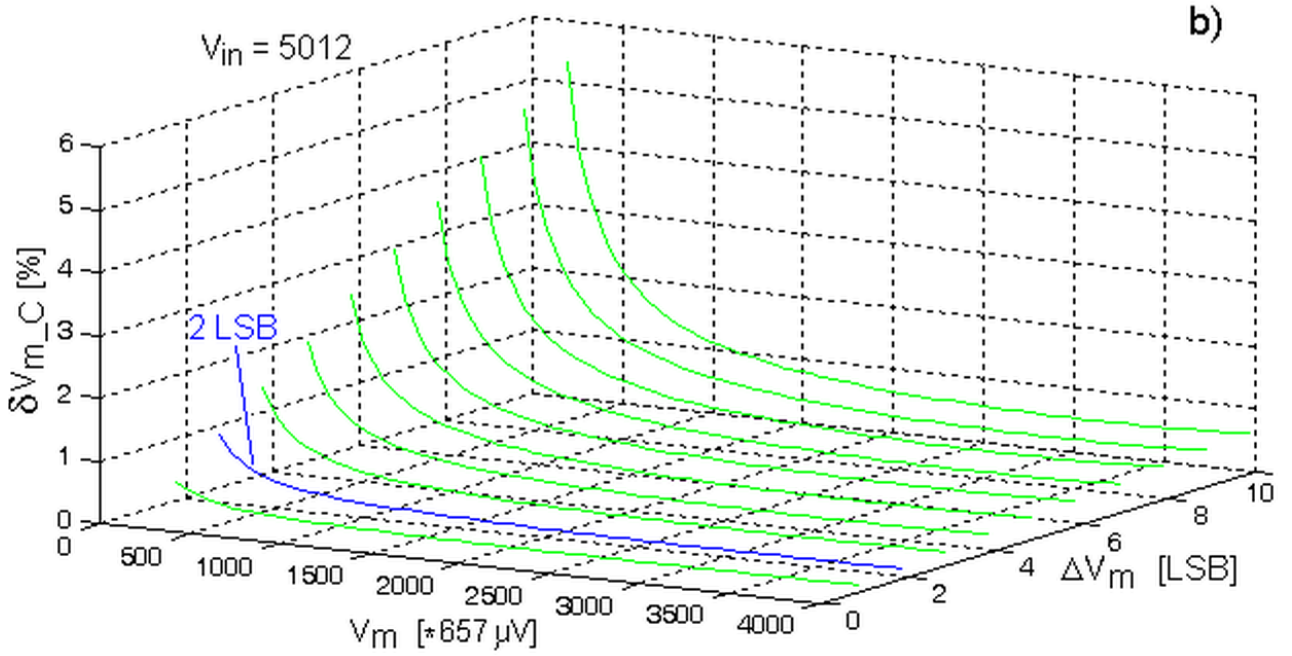

Figure 9

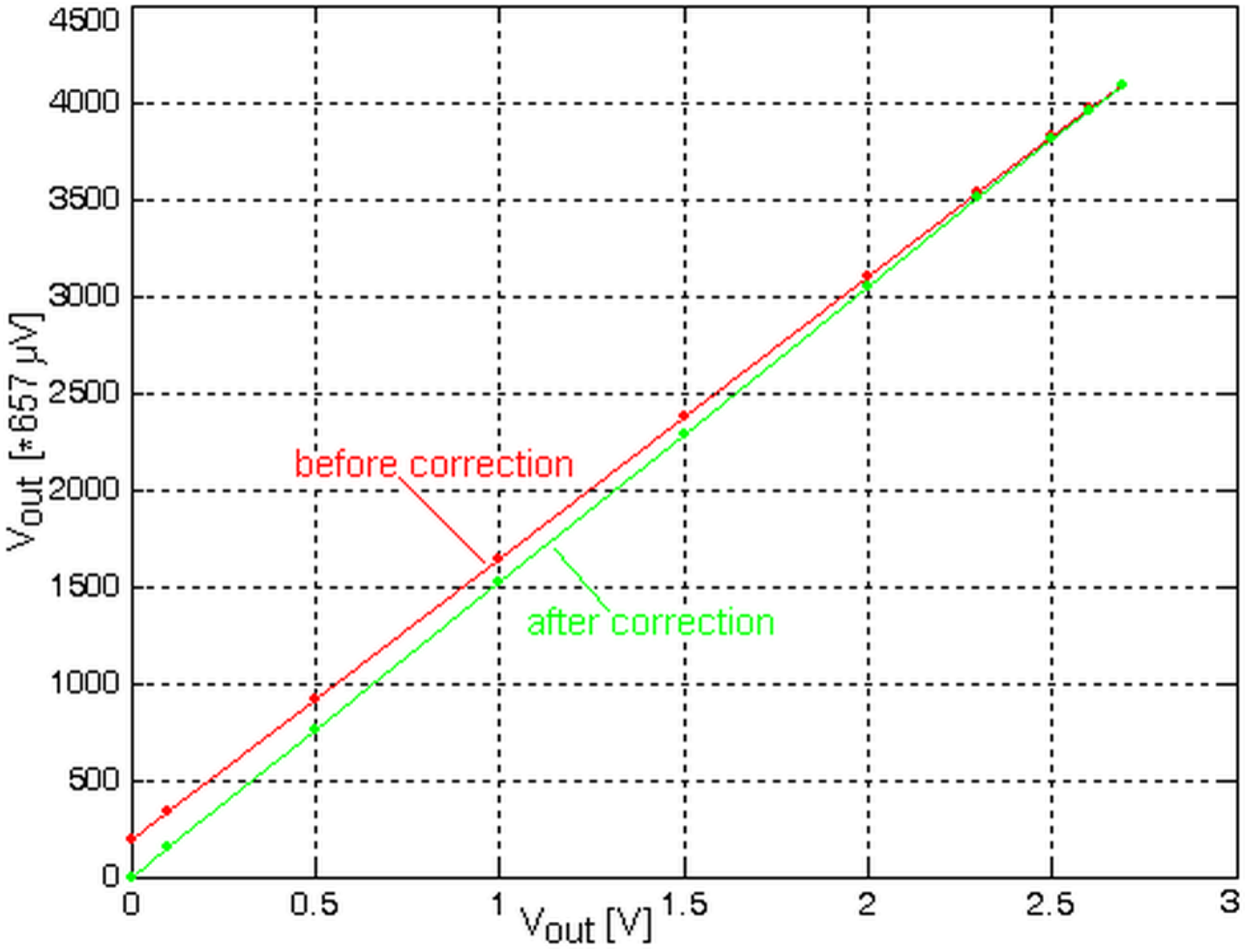

Figure 10

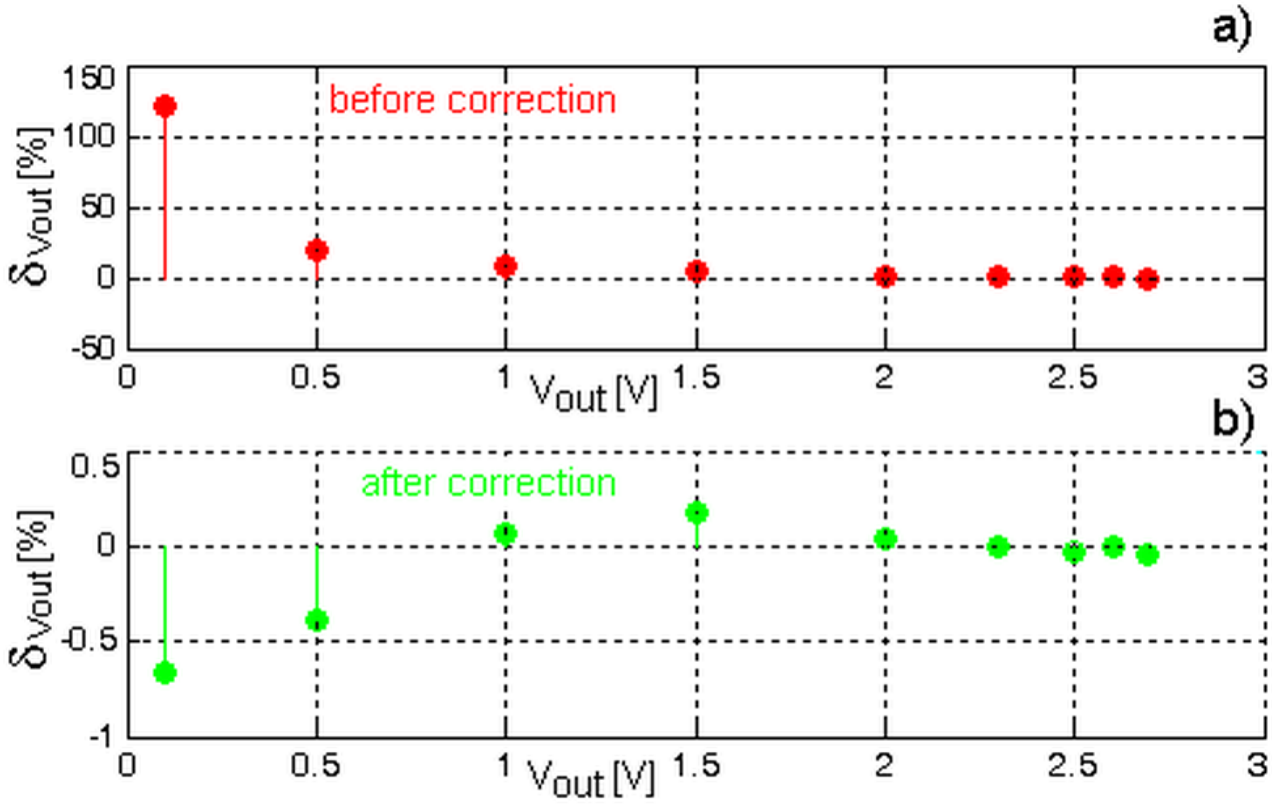

Figure 11

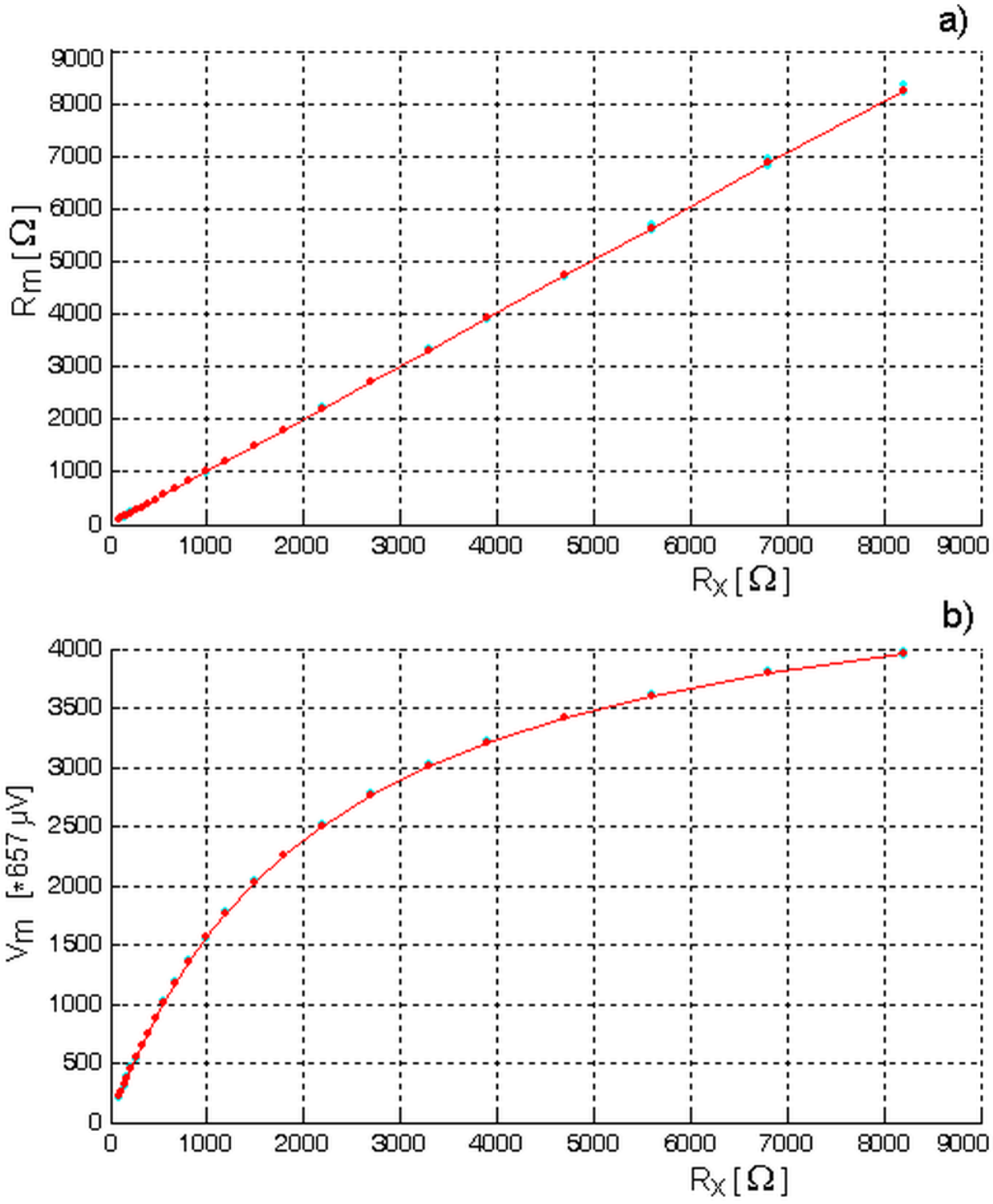

Figure 12

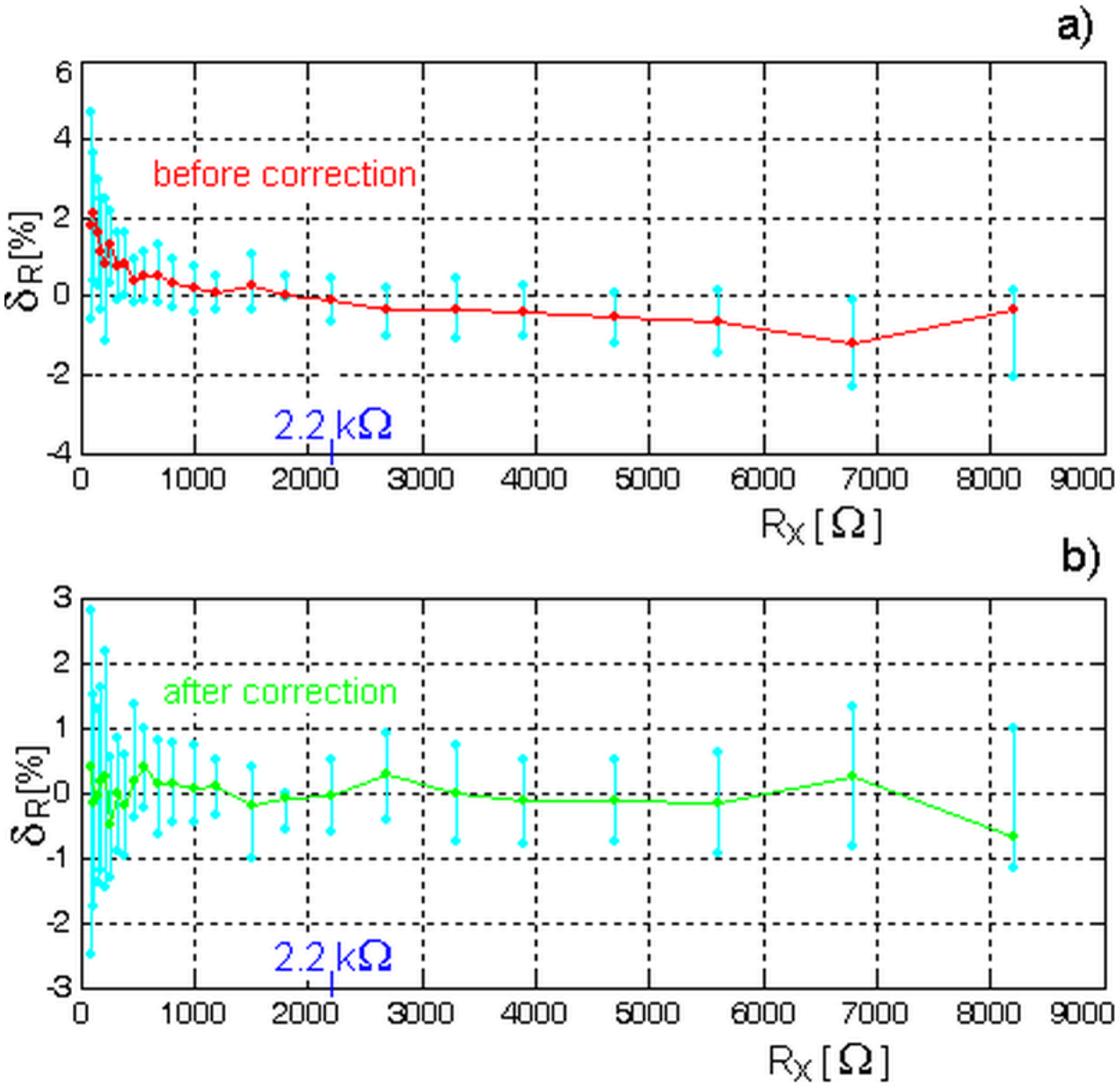

Figure 13

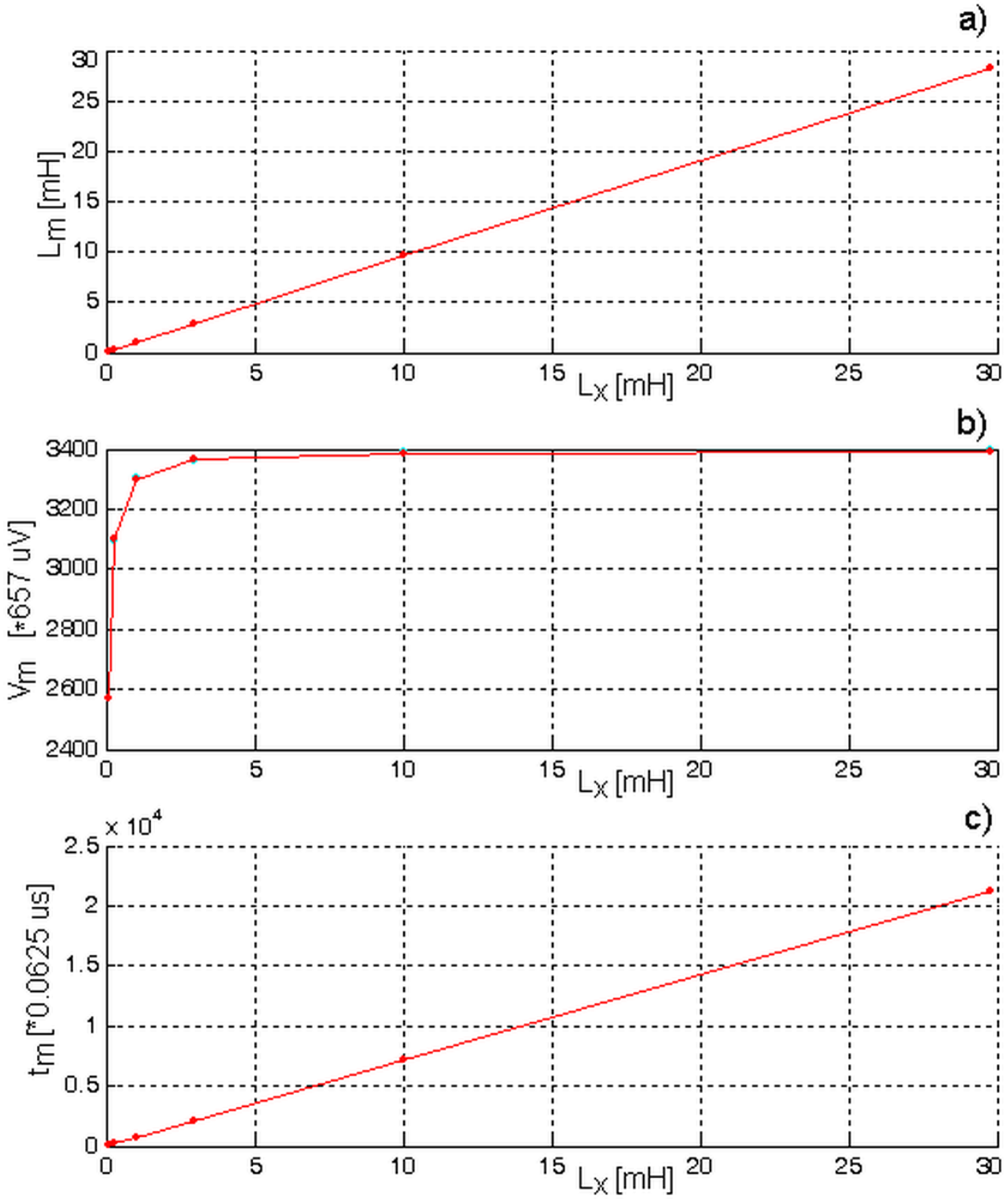

Figure 14

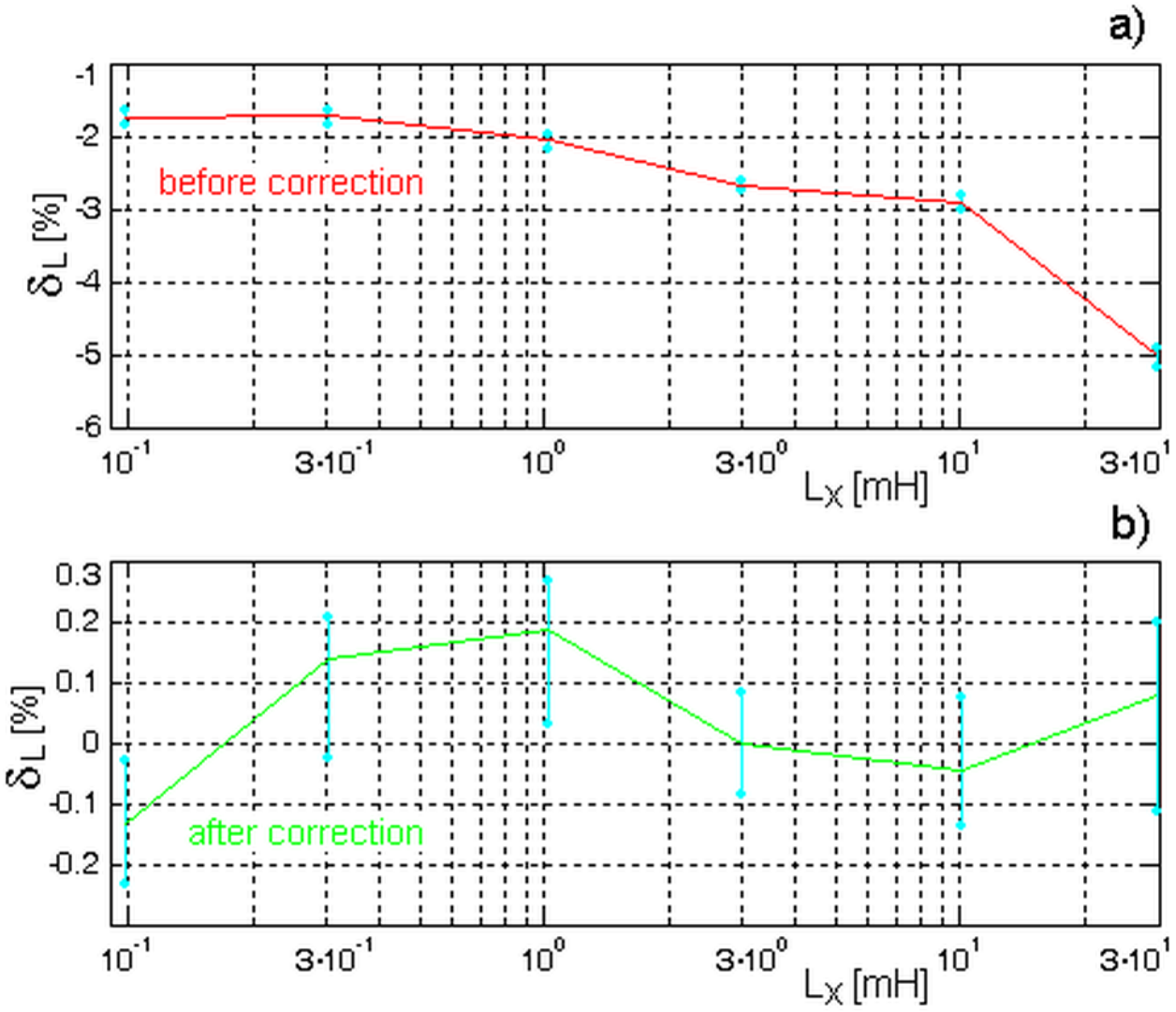

Figure 15

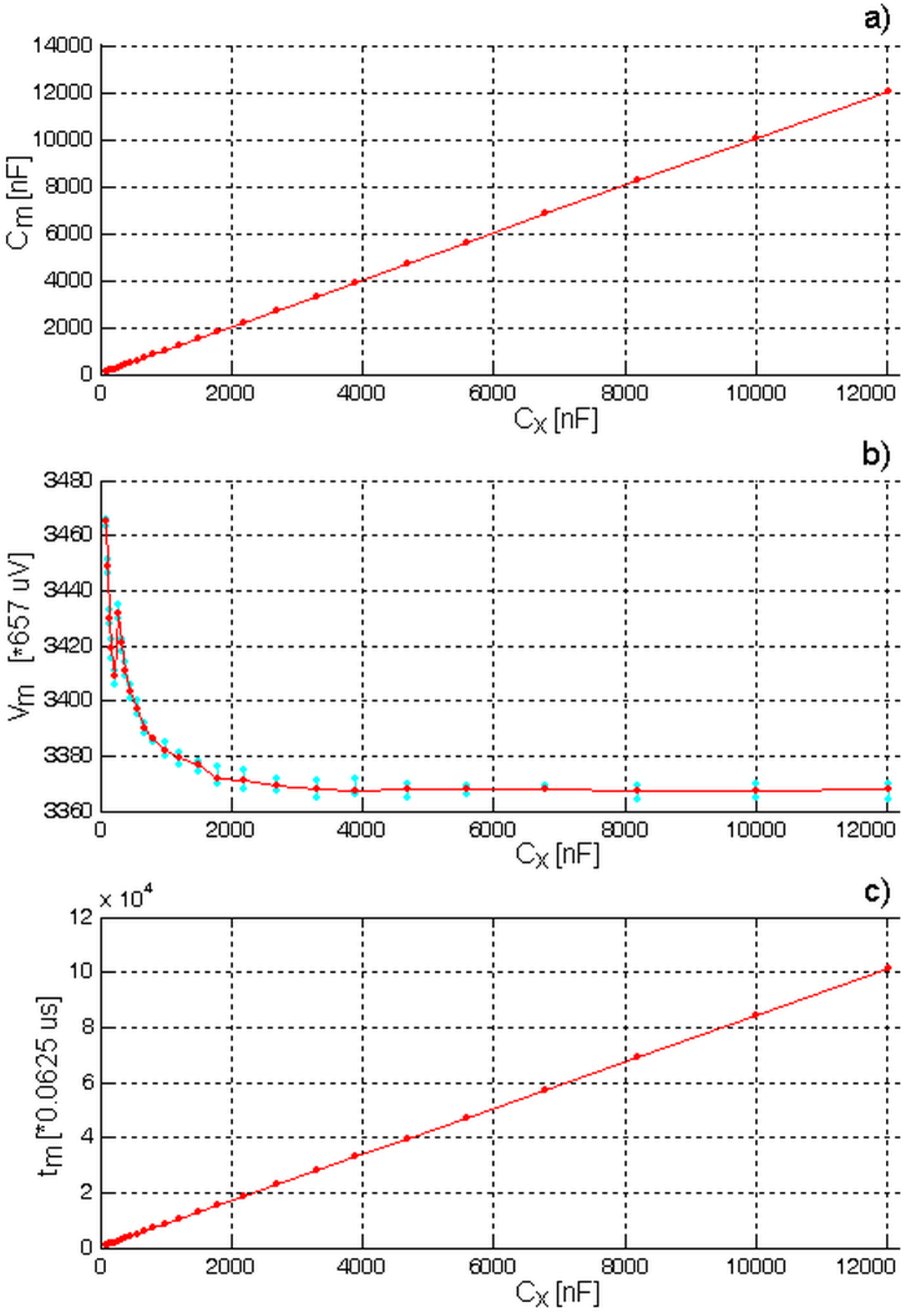

Figure 16